Hindawi
International Journal of Energy Research
Volume 2023, Article ID 5999997, 25 pages
https://doi.org/10.1155/2023/5999997

Research Article

Cascaded Fractional Model Predictive Controller for Load Frequency Control in Multiarea Hybrid Renewable Energy System with Uncertainties

Muhammad Majid Gulzar,[1] **Daud Sibtain**,[2] **and Muhammad Khalid**[3,4]

[1]*Control & Instrumentation Engineering Department & Center for Renewable Energy and Power Systems, King Fahd University of Petroleum & Minerals, Dhahran 31261, Saudi Arabia*
[2]*Department of Electrical Engineering, University of Central Punjab, Lahore, Pakistan*
[3]*Electrical Engineering Department & Center for Renewable Energy and Power Systems, King Fahd University of Petroleum & Minerals, Dhahran 31261, Saudi Arabia*
[4]*SDAIA-KFUPM Joint Research Center for Artificial Intelligence, King Fahd University of Petroleum & Minerals, Dhahran 31261, Saudi Arabia*

Correspondence should be addressed to Muhammad Khalid; mkhalid@kfupm.edu.sa

Received 9 November 2022; Revised 11 January 2023; Accepted 31 January 2023; Published 23 February 2023

Academic Editor: Yogendra Arya

The rapid utilization of electricity has forced the stability of the power system for continuous operation. Due to difference in demand and generation, the frequency reference point changes that needs to be restored to its locus point for the stable operation of the power system. Therefore, a novel efficient control design is propounded to counter the phenomena of load frequency control. The designing of cascaded fractional model predictive controller coupled with fractional-order PID controller (CFMPC-FOPID) is designed for an efficient response of the power system under load disruption and system parameter variations. The controller is optimized by sooty tern optimization algorithm to identify the optimal parameters of the controller. The controller is tested under power mixing of renewable energy sources (i.e., PV and wind) and under varying load scenarios in multiarea hybrid power system. The proposed controller has effectively handled the frequency disruption under distinct load change by stabilizing it in 1.34 sec, 0.60 sec, and 0.41 sec for area-1 with an average time of 0.78 sec, and for area-2, the stabilizing time is 1.40 sec, 0.89 sec, and 0.56 sec with an average time of 0.95 sec, whereas the average time for MPC/PI, DSA-FOPID, GWO: PI-PD, and SCA: FOPI-FOPID is 7.67 sec, 4.68 sec, 1.77 sec, and 4.72 sec, respectively, for area-1 and 6.47 sec, 5.13 sec, 3.45 sec, and 5.02 sec, respectively, for area-2. The outcome result justifies the superiority of the studied technique.

1. Introduction

1.1. Background. In recent time, the modern power system complexity has increased due to integration of renewable energy sources (RES) into the power system. In the modern world, electricity plays an essential role in the evolution of the industrialization process, and for this purpose, the main source of energy was conventional generation, i.e., thermal, furnace oil, and gas [1]. The thermal power plants are used as base-load plants that are independent of weather variations and can become operational whenever required. The development and importance of RES is inevitable because of its positive effects on the climate [2]. Furthermore, RES diversify the energy mix, resulting in greater energy security, but also reduce the carbon footprint of the power sector. It also adds a cheaper source of electric power to the energy

mix, bringing the base price of electricity down. However, these RES of electricity are intermittent and negatively impact the power quality of the system. This is mostly manifested in the form of significant frequency variations in the system. The solution to maintain normal power system frequency is exercised by load frequency control (LFC) irrespective of normal or abnormal operating conditions emerging in the power networks. The LFC also provides the regulatory of the tie-line power flow control among the areas [3, 4].

1.2. Literature Review. To guarantee the stability of the power system, extensive research investment on LFC has been devoted, where different power system structures like single area, multiarea, and deregulated power system are tested for the power system stability [5, 6]. For LFC problem, numerous control techniques are implemented to confirm the continuity of the power system under uncertainty in the power system, i.e., load perturbation or system parameter variations [7]. Over the decades, conventional controlling techniques like proportional-integral (PI) [8], integral (I) [9], and proportional-integral-derivative (PID) controllers are applied in industries due to their easy implementation and low complexity [10]. However, ideality is impossible in a nonlinear system, and some disadvantages are always linked to it; although the PI controller reduces the steady-state error, the drawback of using a traditional PID controller is that it is difficult to find its optimal state due to the trade-off between the derivative and integral parts. Although increasing an integral portion fixes the previous issue, the integral term in the controller causes unwanted behavior during the transitory stage. The existence of an integral term in the transient state improves feedback error by boosting corrective reaction, reducing system stability and speed. A trade-off between derivative and integral gain has become a difficulty for PID controller design to get the greatest performance [11, 12].

In [13], the whale optimization algorithm- (WOA-) centered load frequency PID regulation of renewable energy source was introduced. In [14], the artificial bee colony (ABC) approach was used to improve the values of PI and PID controllers for AGC, and the outcome was compared to particle swarm optimization (PSO). The improved JAYA algorithm-based load frequency management of a power system was investigated in [15]. To address the limitations of conventional methods, such as the sine-cosine algorithm (SCA), the literature study advised the combination of control techniques with newer algorithms [16], bacteria foraging optimization algorithm (BFOA) [17], ant colony optimization (ACO) [18], salp swarm algorithm (SSA) [19], and firefly algorithm (FA) [20]. Moreover, the PID controller is transformed using the property of fractional calculus to extent the range of the conventional PID controller by fractionalizing the integral and derivative controllers [21].

In [22], FOPI controller was formulated with the help of dragonfly search algorithm in multiarea power system. In [23], the flexible structure of FOPID/FOPI/FOI is implemented for automatic generation control (AGC) power system to improve the compatibility of the fractional-order structures. Furthermore, cascaded controller designs, such as PI-PD and PD-PID, using various optimizing algorithms are used in LFC for multiarea power energy system [24, 25]. On a similar note, the designing of cascaded FOPI-FOPID using the optimizing property of sine-cosine algorithm (SCA) is implemented in [26]. The particle swarm optimization (PSO) was exploited for tuning FOPI-FOPD cascaded with fuzzy in [27]. The further modifications in the control structure are designed to expedite the performance of the controller. In [28], fractional-order fuzzy PID controller is presented for LFC in multiarea power system. Similarly, the chaos game optimization (CGO) was implemented to optimize FOPID-FOPI for multiarea power system [29]. Similar to the fractional controller, tilted integral derivative (TID) is also utilized for LFC without filter [30] and with filter [31]. Further in literature review, different sorts of combinations are designed to magnify the controlling ability of the controllers.

In [32], the model predictive controller (MPC) was deployed for thermal-based power system, where the effect of RES was missing. Keeping the limitation in notice, MPC/PI controller was developed in [33], where the penetration of PV was fed to a grid in two-area power system. In addition, multiverse optimizer-tuned MPC was proposed with six RES-based plants in [34]. Likewise, variable structure gain scheduling model predictive controller (GSMPC-PI) was introduced to cope up the LFC problem under renewable-based power system in [35]. The adaptive design for MPC was also proposed in [36], for multiarea power system. Similarly, AMPC controller was formulated to counter frequency oscillations that are perturbed due to load disturbance in a hybrid power system [37]. In recent time, designing of master-slave (MS) controller is developed for multiarea power system in which the LFC and fault affects in the power system are investigated [38].

1.3. Research Gap and Motivation. After an in-depth literature review, many control practices are investigated to counter the frequency oscillations in the power system. The power system faces many challenges in terms of frequency and continuity of the power flow. Ensuring the stability of the power system is indispensable by sustaining the frequency to its nominal operating value. However, these challenges amplify when RES (PV and wind) are incorporated in the power system with high penetration. From the aforementioned literature review, different control techniques are examined, but the complexity (incorporation of RES) is limited. The number of control techniques has been applied in addressing the challenge of LFC. But cascaded based MPC formations/structures are less focused in the literature, and most of the studies are ignoring the impact of renewable into the AGC of deregulated power system.

1.4. Challenges. The system frequency and tie flows deviate from their expected values because of oscillations in load demand, which in turn produces disparities between generation and demand. The primary obstacles in the way of a solution to this issue are as follows:

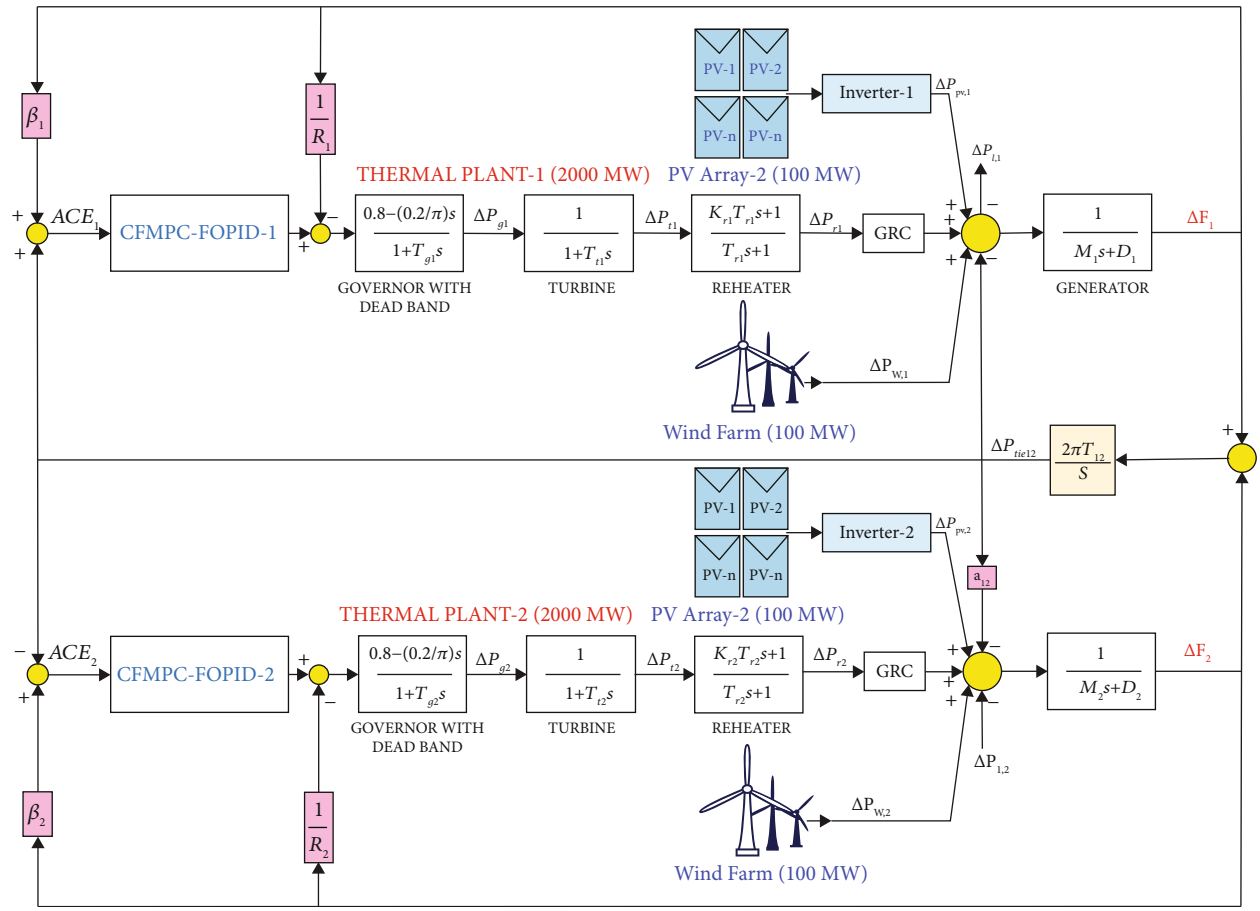

Figure 1: Two-area model under study.

(i) Utilizing a novel AGC controller to efficiently mitigate out-of-bound fluctuations in system frequency, generation, and tie-line flows

(ii) The proposed controller should have the robust tendency to achieve the rapid response in terms of minimum settling time, undershoot, and overshoot

(iii) The tunable parameters are to be adjusted by a suitable optimizing algorithm for optimal operation of the designed controller

(iv) The proposed technique should outperform the existing control technique by overcoming the challenges in a robust way

1.5. Contribution. The main contribution and innovation of this paper are highlighted as follows:

(i) This study proposes a modified cascaded design, where the fractional design of MPC coupled with FOPID (CFMPC-FOPID) controller is implemented for frequency regulation in a renewable-designed AGC-deregulated power system

(ii) The refine tuning of the controller is achieved by the sooty tern optimization algorithm (STOA). Through the help of STOA, the parameters of MPC and dual FOPID-1 and coupled FOPID-2 are tuned to minimize the ITAE

(iii) The efficiency of the suggested controller is verified under multiarea power system incorporating PV and wind into the grid. Under the tested system, the proposed controller has revealed robust results as compared to DSA-FOPI [22], GWO: PI-PD [24], SCA: FOPI-FOPID [26], and MPC/PI [33]

(iv) Effective performance evaluation tests are performed to ensure the robustness of the proposed design. The changing load scenario tests are applied, the nonlinearity of the system test is evaluated, and a sensitivity analysis has been established

(v) Lastly, the overall stability of the system has been conducted under the proposed controller design, while the main innovative idea contributes around the CFMPC-FOPID design and its effectiveness to ensure the robust operation for the AGC-deregulated power system

1.6. Organization of the Paper. The organization of the paper is ordered as follows: The discussion of power system is explained in section "Multi area hybrid power system". The proposed controller is displayed in section "Designing

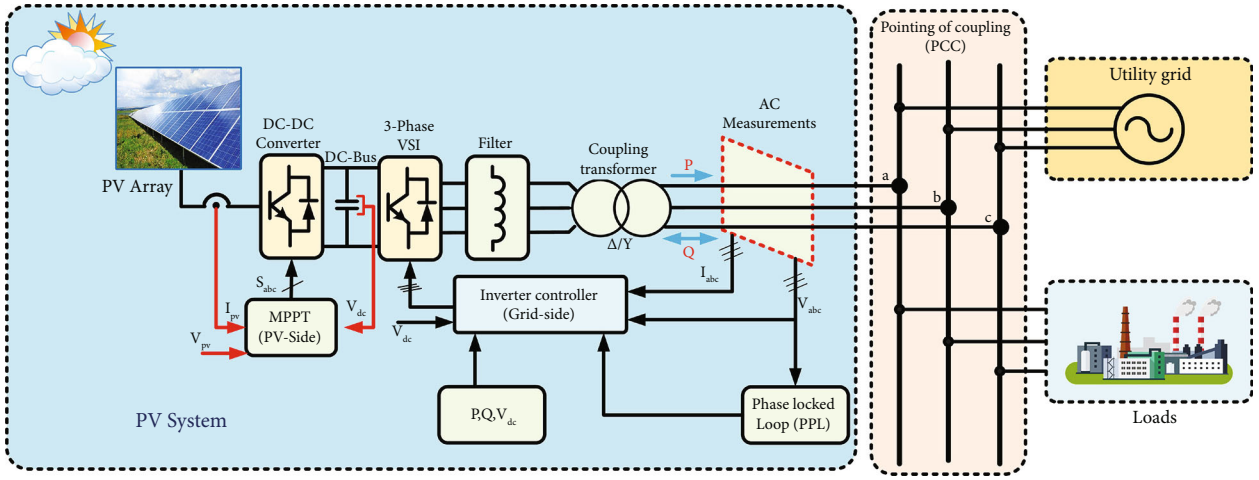

Figure 2: PV grid model.

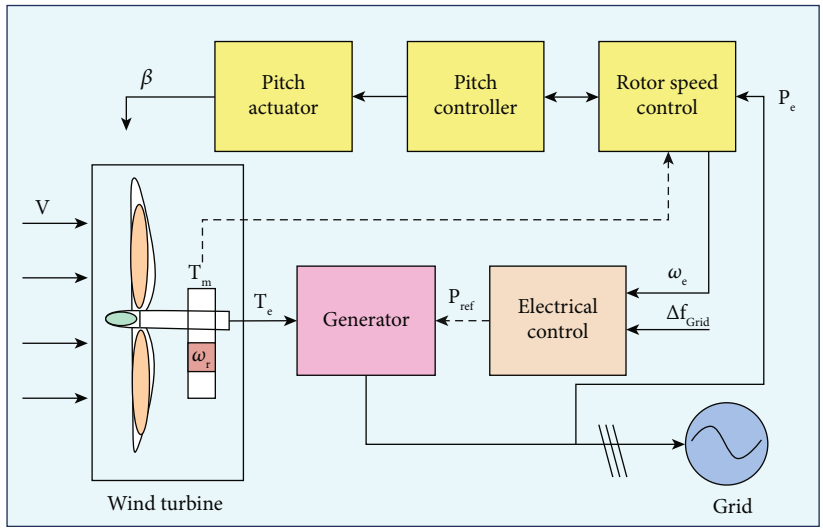

Figure 3: Wind power system schematic.

of CFMPC-FOPID". The effectiveness of the controller is discussed in section "Results and discussion". Finally, the crux of the paper is translated in Conclusion.

2. Two-Area Hybrid Power System

In a two-area electrical network, each region has a thermal power system and incorporates PV and wind. The connection of two areas is formed by a tie-line from where the power sharing between two areas take place. The two-area hybrid power system is depicted in Figure 1. The detailed modelling of the two-area hybrid power system is explained in upcoming portion.

2.1. PV System Designing. As the world transition towards RES is expediting, thus PV systems are extensively utilized. An equivalent model of a solar cell entails of a parallel current source and a diode, rendering it a nonlinear energy source. The series-parallel arrangement of solar cells produces a solar panel. These solar panels are then applied to generate solar-powered electricity. The variations in irradiance and temperature will alter the module's current and voltage, correspondingly. Owing to in-built nonlinear property of the PV module, it is necessary to form such a system that works on MPPT so that supreme power can be extracted. The design of the solar PV is carried out at maximum power point with 1000 W/m^2 at 25°C. [38]. The PV model contains the converter for achieving the MPPT, while inverter plays an important role in converting DC into AC source for satisfying the AC-based power systems. The PV-connected grid model is presented in Figure 2. The MPP of this solar array connection is at $I = 750$ A, which corresponds to an MPP of 4.5 MW. This is adequate for the current application, as the thermal power system maximum load is 1000 MVA.

The model is designed for a capacity of 30 kW penetrating at a level of 45% into the grid. The gain between AC and DC is derived from

$$X = \frac{V\mathrm{dc}}{V\mathrm{ac}}, \tag{1}$$

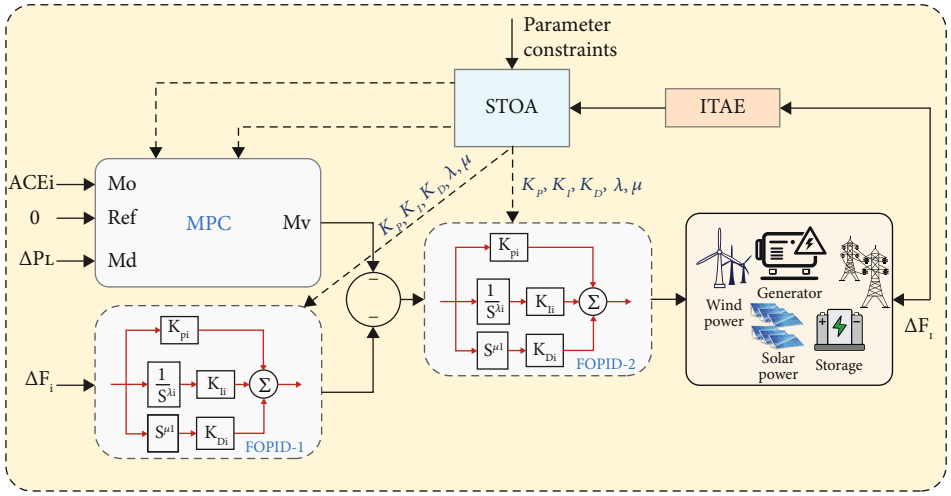

Figure 4: CFMPC-FOPID controller design.

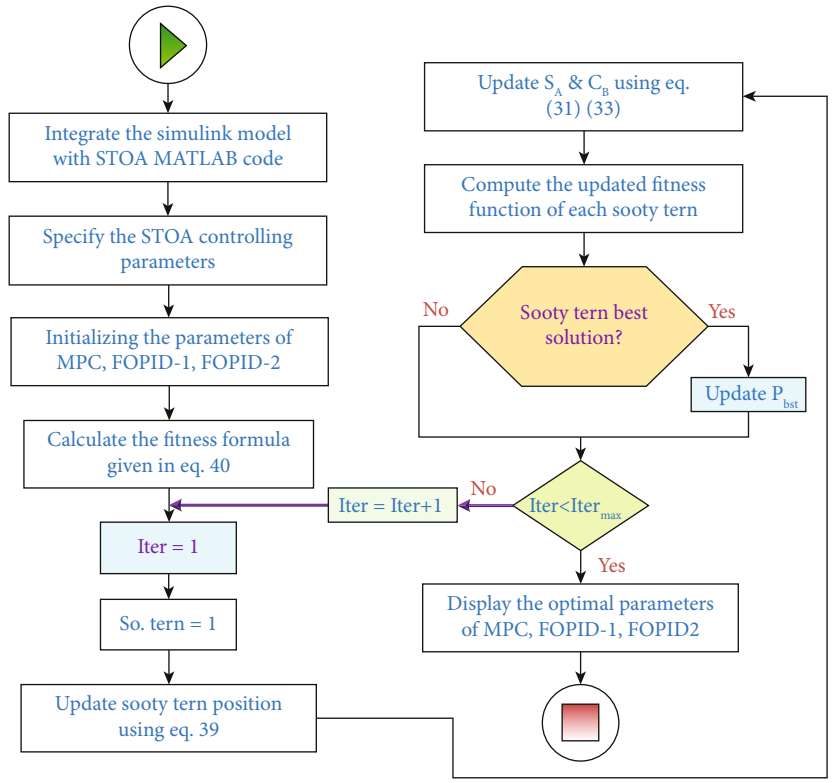

Figure 5: STOA flow chart for CFMPC-FOPID controller.

where X presents the gain between AC and DC values which selected as 0.7. The constant dc voltage $V_{dc} = 6\,\text{kV}$, where PV operates. Since this DC value is constant, by selecting X for this particular system, the amplitude of the AC voltage remains constant, but the AC current and power fluctuate with the DC value.

The required voltage after the boost converter is obtained by the V_o as mentioned in

$$V_o = \frac{V_{AC,rms}}{X} = \frac{11/\sqrt{3}}{0.7} = 9.07\,\text{kV}. \tag{2}$$

Therefore, the calculation of boost converter gain is expressed in equation (3), and final boost converter gain is represented in equation (4).

$$M = \frac{V_o}{X} = \frac{9.07\,\text{kV}}{6\,\text{kV}} = 1.51, \tag{3}$$

$$G_{\text{Boost}} = \frac{1}{M} = \frac{1}{1.51}. \tag{4}$$

After designing of the boost converter gain, the next step is to find the inverter transfer function for the

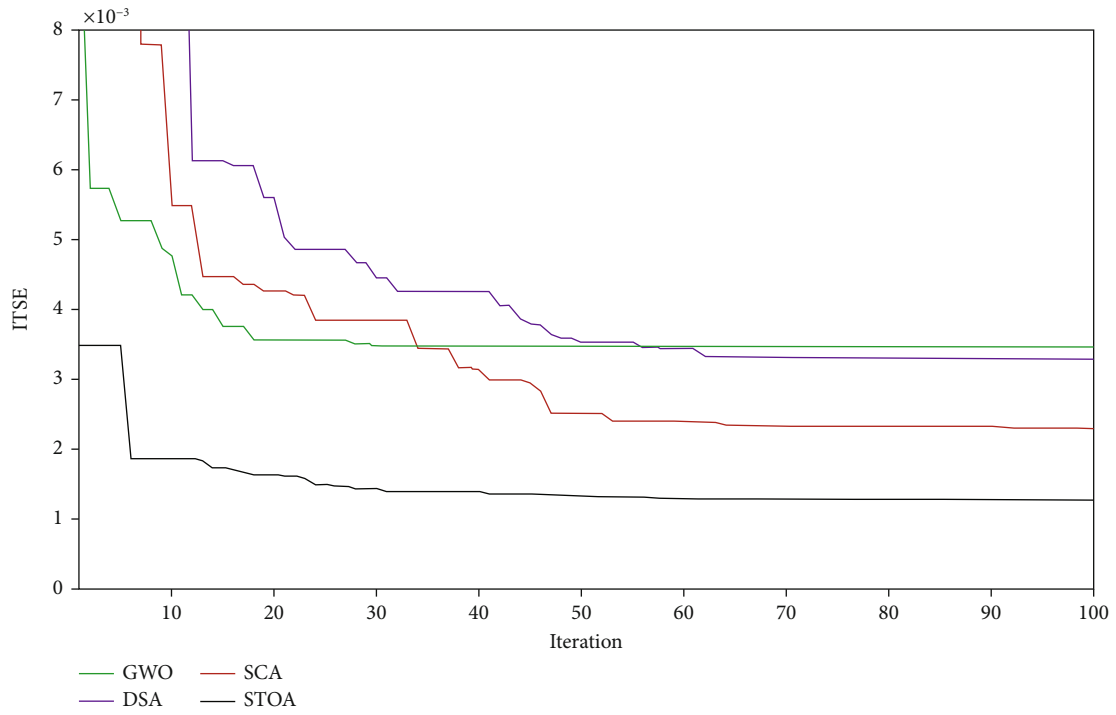

Figure 6: Algorithm convergence analysis.

Table 1: Optimal parameters of different controller at 100 iterations.

Multiarea	SCA: FOPI-FOPID [26]	GWO: PI-PD [24]	DSA-FOPI [22]	MPC/PI [33]	Proposed controller
Area-1	$K_{P1} = 0.0216$ $K_{I1} = 0.580$ $\lambda_1 = 0.891$ $K_{P12} = 0.1061$ $K_{I12} = 0.8139$ $K_{D12} = 0.0311$ $\lambda_{12} = 0.679$ $\mu_{12} = 0.081$	$K_{P1} = -3.018$ $K_{I1} = -2.167$ $K_{P1} = -2.501$ $K_{D1} = -1.012$	$K_P = 1.207$ $K_I = 5.199$ $K_D = 0.289$ $\lambda = 0.699$	$K_P = 0.301$ $K_I = 0.870$	$K_{P1} = 2.110$ $K_{I1} = 4.122$ $K_{D1} = 0.0281$ $\lambda_1 = 0.991$ $\mu_1 = 0.809$ $K_{P2} = 1.652$ $K_{I2} = 3.788$ $K_{D2} = 0.0382$ $\lambda_2 = 0.728$ $\mu_2 = 0.791$ MPC parameters $P = 10$ $M = 2.357$ $R = 3.895$ $Q = 1.000$
Area-2	$K_{P2} = 0.0408$ $K_{I2} = 0.3111$ $\lambda_2 = 0.607$ $K_{P22} = 0.0871$ $K_{I22} = 0.9024$ $K_{D22} = 0.0732$ $\lambda_{22} = 0.841$ $\mu_{22} = 0.974$	$K_{P1} = -2.019$ $K_{I1} = -3.022$ $K_{P1} = -3.514$ $K_{D1} = -0.828$	$K_P = 0.873$ $K_I = 5.158$ $K_D = 1.991$ $\lambda = 0.801$	$K_P = 0.196$ $K_I = 0.827$	$K_{P1} = 1.933$ $K_{I1} = 5.281$ $K_{D1} = 0.0301$ $\lambda_1 = 0.902$ $\mu_1 = 0.930$ $K_{P2} = 0.885$ $K_{I2} = 2.551$ $K_{D2} = 0.0112$ $\lambda_2 = 0.898$ $\mu_2 = 0.995$ MPC parameters $P = 6$ $M = 4.237$ $R = 5.285$ $Q = 1.003$

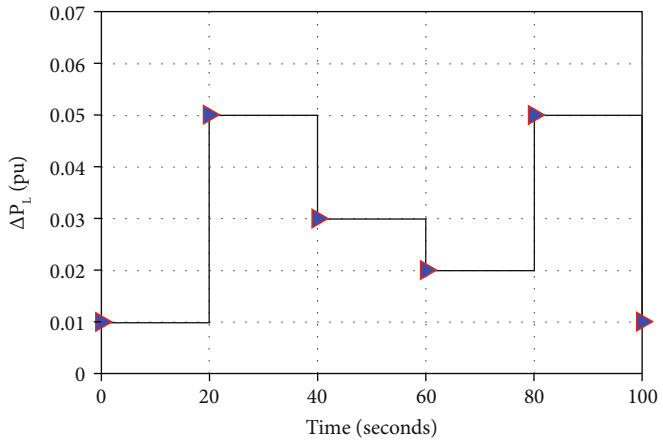

Figure 7: Similar load changing pattern in multiarea.

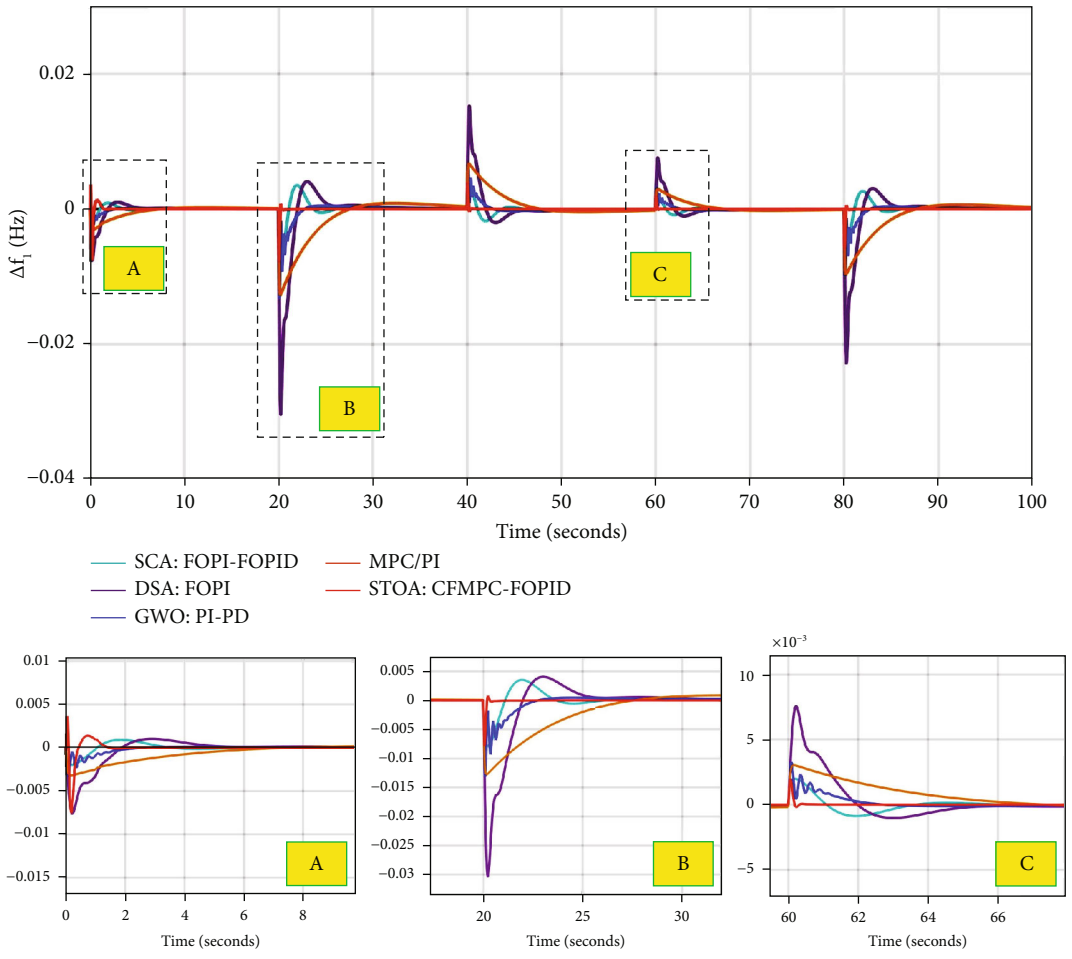

Figure 8: Frequency deviation response in area-1.

conversion of DC current into AC current. The AC current is given by $i_{ac} = I_m \cos \omega t$, and its equivalent transfer function is signified by $s/(s^2 + \omega^2)$, where $\omega = 2\pi f = 2(3.14)(50) = 314.159$ rad/sec.

The transfer function of the inverter is the output current of the inverter to the input current of the inverter. The input current to the inverter is the output DC current of the boost converter that is denoted by $1/s$. The representation of the inverter transfer function is given in

$$G_{\text{Inverter}} = \frac{i_{ac}}{i_{\text{input}}} = \frac{s}{s^2 + \omega^2} \div \frac{1}{s} = \frac{s}{s^2 + \omega^2} = \frac{s}{s^2 + 98700}. \tag{5}$$

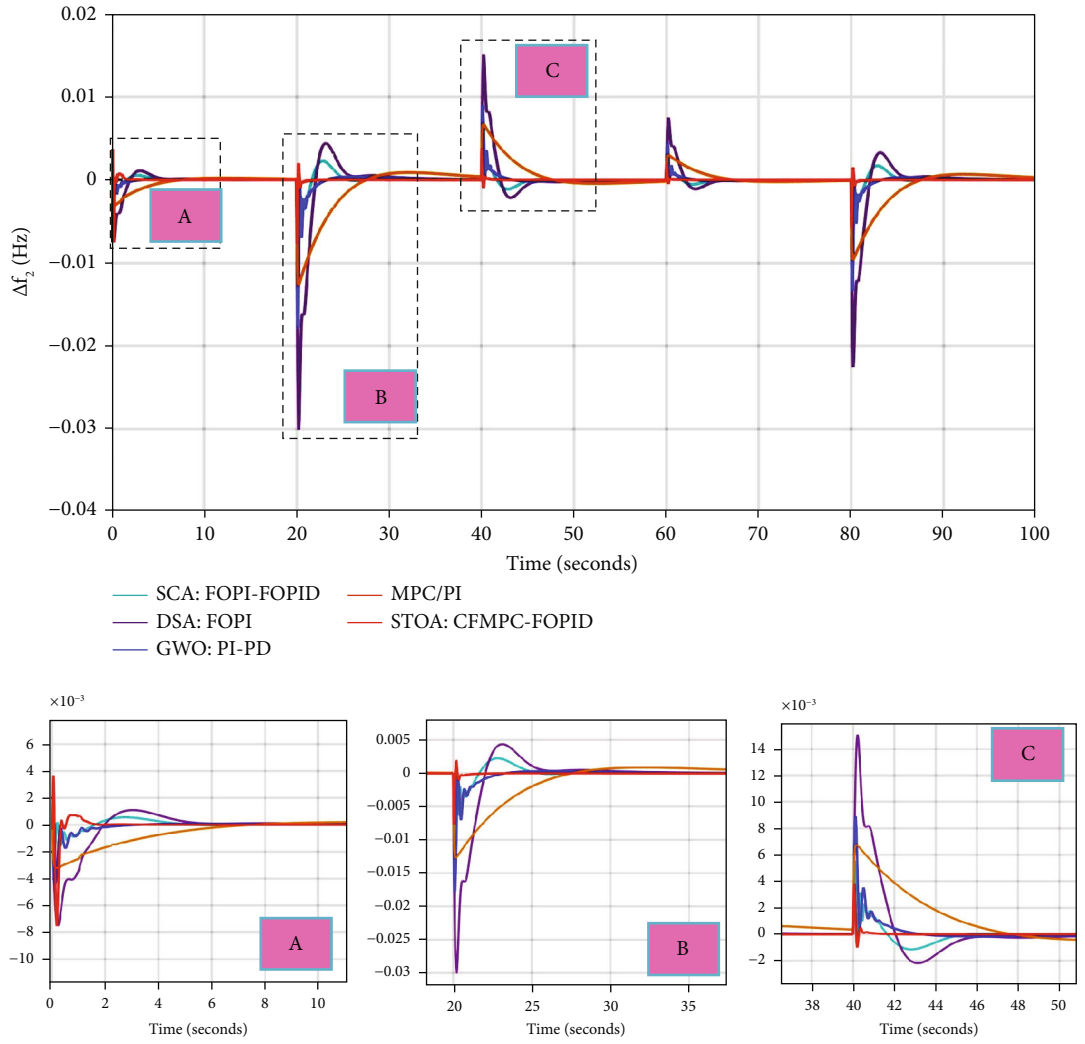

Figure 9: Frequency deviation response in area-2.

Table 2: Controller analysis in area-1 for Point-A, Point-B, and Point-C on graph under similar load condition.

Controllers	Area-1 Point-A			Point-B			Point-C		
	S.T (s)	U.S (Hz)	O.S (Hz)	S.T (s)	U.S (Hz)	O.S (Hz)	S.T (s)	U.S (Hz)	O.S (Hz)
Proposed	1.21	0.0068	0.0031	0.727	0.0062	0	0.689	0	0.0032
MPC/PI [33]	7.89	0.0042	0	11.58	0.014	0.0010	5.728	0	0.0044
DSA-FOPID [22]	5.67	0.0065	0.0020	5.308	0.03	0.00431	5.211	0.00129	0.00785
GWO: PI-PD [24]	1.98	0.0052	0	2.89	0.0098	0	2.014	0	0.00304
SCA: FOPI-FOPID [26]	3.047	0.0041	0.0019	5.101	0.0079	0.048	3.108	0.00108	0.00312

As the output fed to the grid from the PV source is in the form of power, thus the instantaneous power $p(t)$ is given in

$$p(t) = \frac{V_m}{I_m} i^2_{\mathrm{AC}}. \tag{6}$$

In equation (6) the V_m/I_m is representing real part of the impedance because of the purely resistive load, and further taking the Laplace transformation of equation (6), it is translated in

$$P(s) = \frac{V_m I_m}{2s} + \frac{V_m I_m}{2s} \frac{s}{s^2 + (2\omega)^2}. \tag{7}$$

Transforming the AC current into instantaneous power transfer function is given by

Table 3: Controller analysis in area-2 for Point-A, Point-B, and Point-C on graph under similar load condition.

Controllers	Area-2 Point-A S.T (s)	Point-A U.S (Hz)	Point-A O.S (Hz)	Area-2 Point-B S.T (s)	Point-B U.S (Hz)	Point-B O.S (Hz)	Area-2 Point-C S.T (s)	Point-C U.S (Hz)	Point-C O.S (Hz)
Proposed	1.79	0.0072	0.0038	0.651	00.0061	0.0011	0.86	0.0008	0.0038
MPC/PI [33]	6.708	0.0035	0	7.88	0.013	0	9.087	0	0.0065
DSA-FOPID [22]	5.71	0.0076	0.0011	6.08	0.03	0.00480	5.701	0.0020	0.0148
GWO: PI-PD [24]	2.08	0.0041	0	2.72	0.0161	0	3.211	0	0.0090
SCA: FOPI-FOPID [26]	4.022	0.0038	0.0008	5.09	0.0036	0.037	4.801	0.00137	0.00332

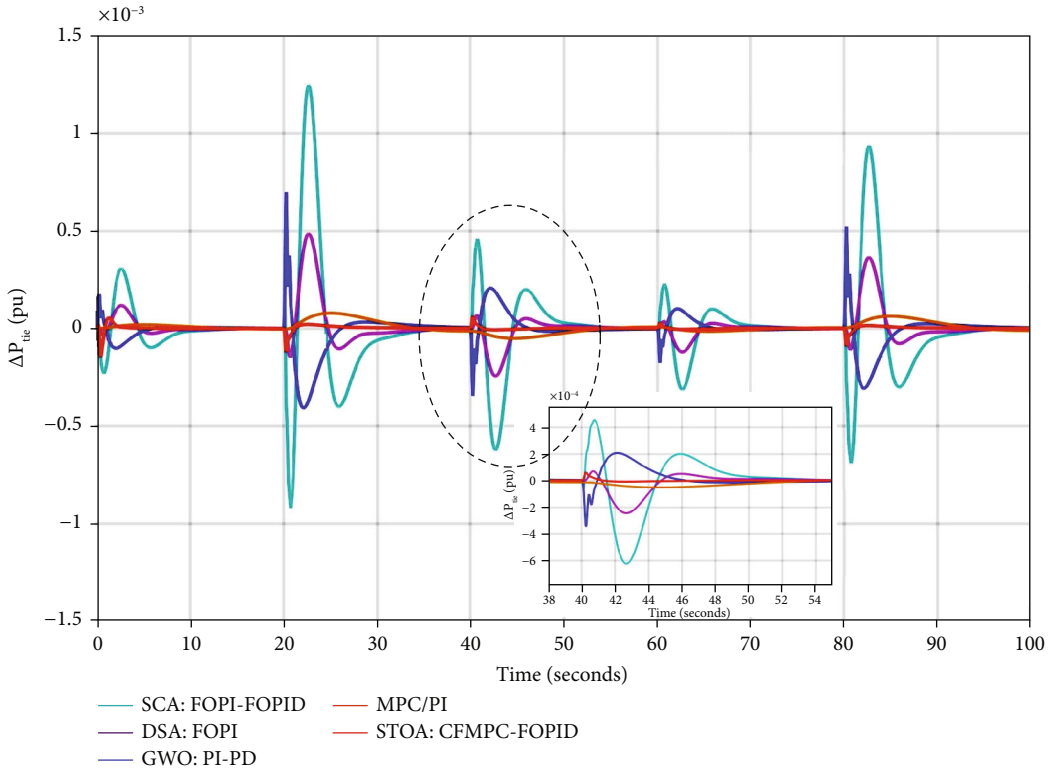

Figure 10: Power sharing response between the two areas under similar load.

$$G_{\text{inst}}(s) = \frac{P(s)}{i_{\text{ac}}(s)} = V_m\left(\frac{\left(s^2+\omega^2\right)\left(s^2+(2\omega)^2\right)}{s^2\left(s^2+(4\omega)^2\right)}\right) = \frac{6351s^4+\left(1.88\times10^9\right)s^2+\left(1.237\times10^{14}\right)}{s^4+\left(3.948\times10^5\right)s^2}. \tag{8}$$

The average power from the instantaneous power gives an average transfer function represented in

$$G_{\text{avg}}(s) = \frac{P_{\text{avg}}(S)}{P(S)} = \frac{\left(S^2+(4\,\text{W})^2\right)}{2\left(S^2+(2\,\text{W})^2\right)} = \frac{s^2+\left(3.948\times10^5\right)}{2s^2+\left(3.948\times10^5\right)}. \tag{9}$$

The 4.5 MW is an average output power from the PV source at which the system is designed.

2.2. Wind System Scheming. Keeping in view the sustainable operation of the power system, the importance of wind power system cannot be ignored as it provides green energy that is environmentally friendly. As the wind strikes the object in this case the windmill, it exerts a force on the propeller-like blades that urges the windmill to move in the direction of the wind. The wind schematic diagram is shown in Figure 3.

The shaft of the windmill is connected with the turbine, and it converts the kinetic energy of the wind into mechanical energy. Just like solar, wind power plants are also an intermittent source of energy because someone cannot control the speed of the air, it all depends on the weather conditions, and the nonlinearity of the wind speed according to the geographical location of the power plant. The output wind power equation that drives the rotation of the windmill is prescribed in [39]

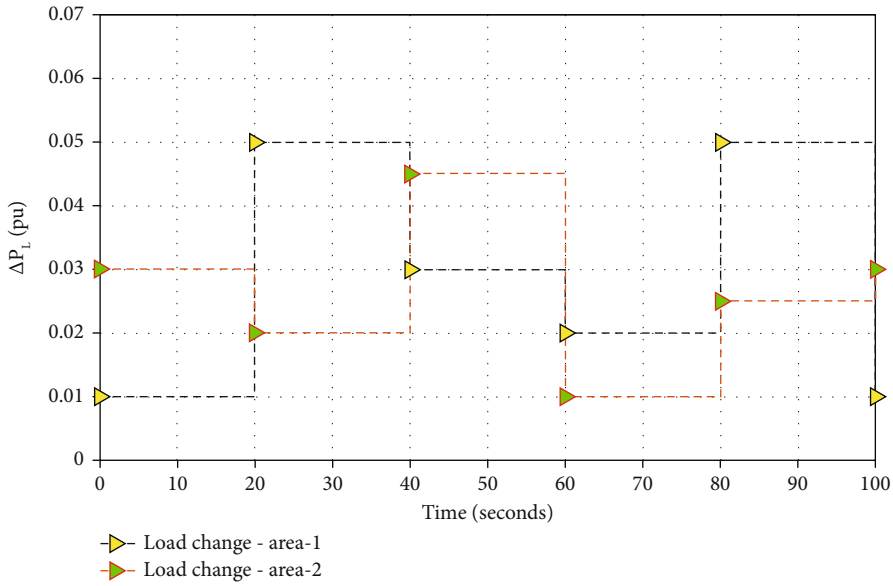

Figure 11: Distinct load changing pattern in multiarea.

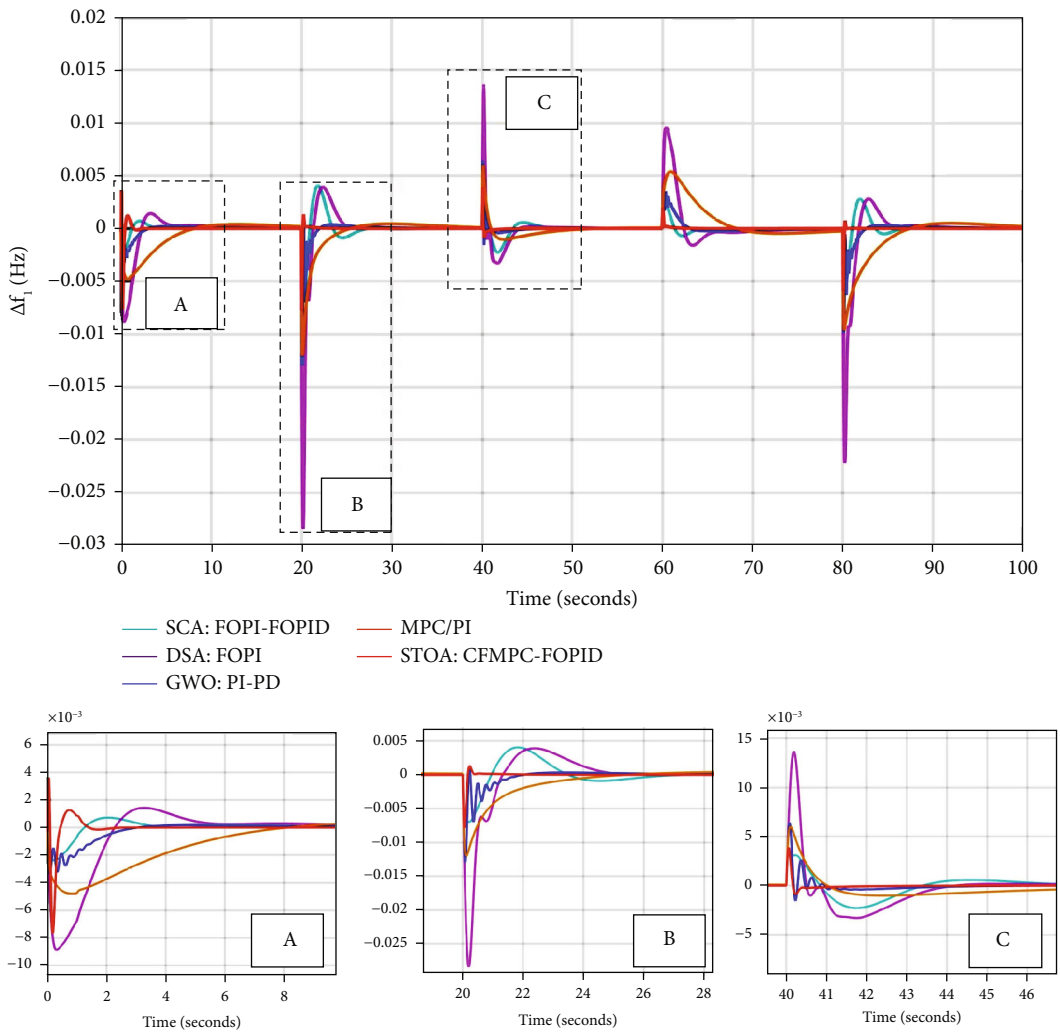

Figure 12: Frequency deviation response under distinct load condition in area-1.

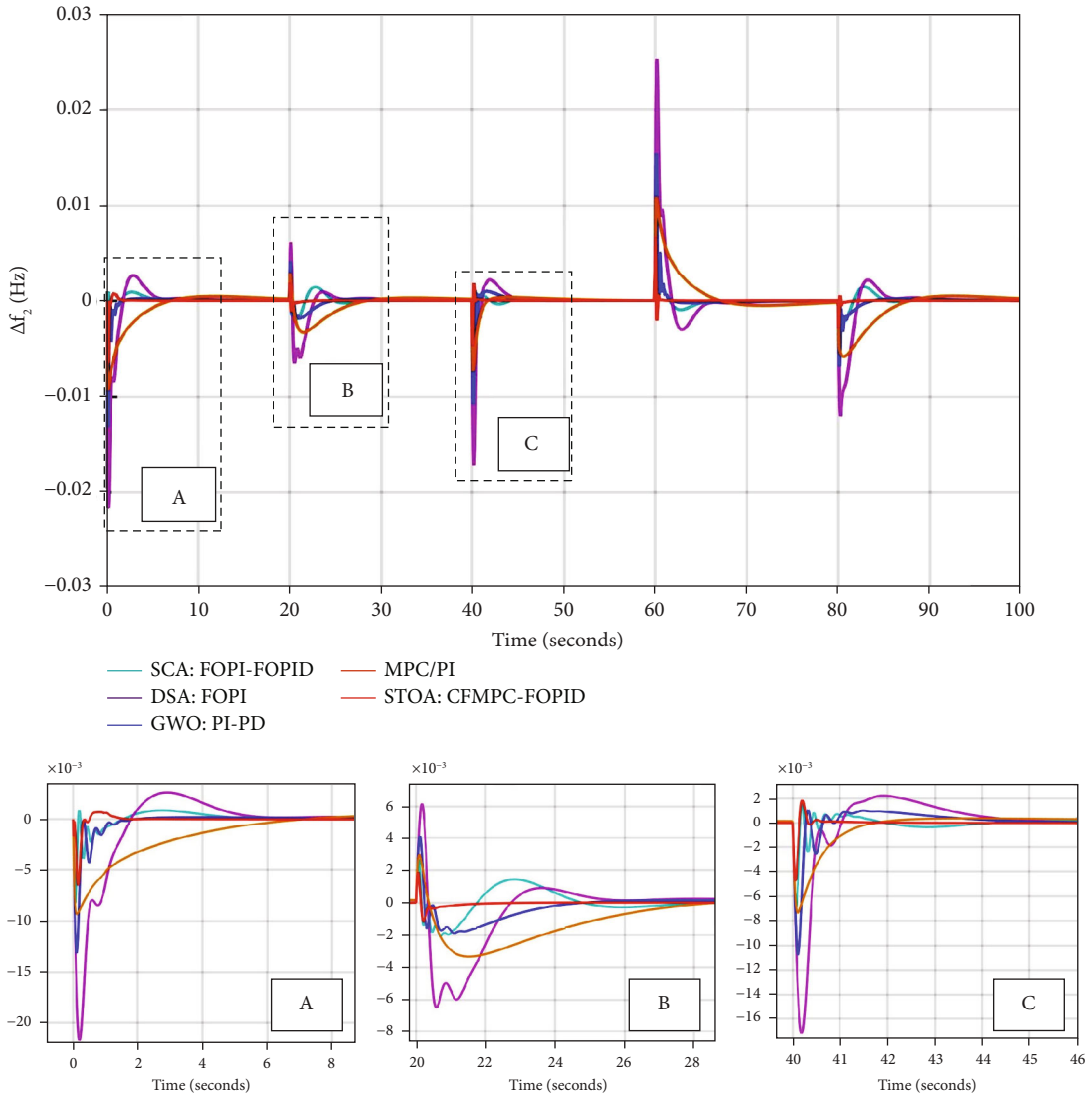

Figure 13: Frequency deviation response under distinct load condition in area-2.

$$P_w = \frac{1}{2}\rho a^2 V_w^3 C_p(\mathrm{TSR}, \beta). \tag{10}$$

The parameters in equation (10) are described as follows: ρ indicates the air density (kg/m^3), C_p signifies the power coefficient, blade pitch angle is represented by β (deg), a (m^2) represents swept area, TSR is turn speed ratio, and V_m (m/s) is the wind speed.

$$C_p = 0.5\left(\mathrm{TSR} - 0.222\,\beta^2 - 5.6\right)e^{-0.17\mathrm{TSR}}, \tag{11}$$

$$\mathrm{TSR} = \frac{\mathrm{rpm} \times \pi D}{60V}, \tag{12}$$

where blade rotor diameter, rotor speed, is denoted by D (m) and rpm (rev/min), respectively. The wind farm includes number of wind turbines where the total capacity of the wind farm is 33 MW. The modelling of the wind farm system representing pitch control, pitch actuator, and induction generator transfer functions is mentioned in [40]

$$G_P(s) = \frac{K_{P1}(1 + sT_{P1})}{(1 + s)}, \tag{13}$$

$$G_H(s) = \frac{K_{P2}}{(1 + sT_{P2})}, \tag{14}$$

$$G_D(s) = \frac{K_{P3}}{(1 + sT_{P3})}, \tag{15}$$

$$G_I(s) = \frac{1}{(1 + sT_w)}. \tag{16}$$

2.3. Thermal Power Modelling. Components of a thermal power plants include an electrical generator, a governor, a steam turbine, and a reheater. The governor of the generator plays an indispensable role in controlling the frequency

Table 4: Controller analysis in area-1 for Point-A, Point-B, and Point-C on graph under distinct load condition.

Controllers	Area-1 Point-A S.T (s)	Point-A U.S (Hz)	Point-A O.S (Hz)	Point-B S.T (s)	Point-B U.S (Hz)	Point-B O.S (Hz)	Point-C S.T (s)	Point-C U.S (Hz)	Point-C O.S (Hz)
Proposed	1.34	0.0077	0.0038	0.601	0.006	0	0.410	0	0.0031
MPC/PI [33]	7.98	0.0050	0	5.051	0.015	0	9.985	0.0009	0.0052
DSA-FOPID [22]	5.13	0.0087	0.0018	4.981	0.034	0.00401	3.928	0.00301	0.01381
GWO: PI-PD [24]	2.312	0.00557	0	2.00	0.0128	0	1.011	0	0.00289
SCA: FOPI-FOPID [26]	3.126	0.00308	0.0012	6.005	0.0061	0.047	5.027	0.00201	0.01302

Table 5: Controller analysis in area-2 for Point-A, Point-B, and Point-C on graph under distinct load condition.

Controllers	Area-2 Point-A S.T (s)	Point-A U.S (Hz)	Point-A O.S (Hz)	Point-B S.T (s)	Point-B U.S (Hz)	Point-B O.S (Hz)	Point-C S.T (s)	Point-C U.S (Hz)	Point-C O.S (Hz)
Proposed	1.401	0.0062	0.0007	0.891	0.001	0.0018	0.560	0.0046	0.0018
MPC/PI [33]	6.87	0.0091	0	7.631	0.038	0	4.902	0.0072	0.00018
DSA-FOPID [22]	5.60	0.0297	0.0039	5.68	0.00612	0.00603	4.108	0.017	0.0021
GWO: PI-PD [24]	1.809	0.00601	0	5.01	0.0022	0.0038	3.521	0.0102	0.001
SCA: FOPI-FOPID [26]	4.028	0.00308	0.00015	7.010	0.0021	0.00187	4.019	0.00611	0.01302

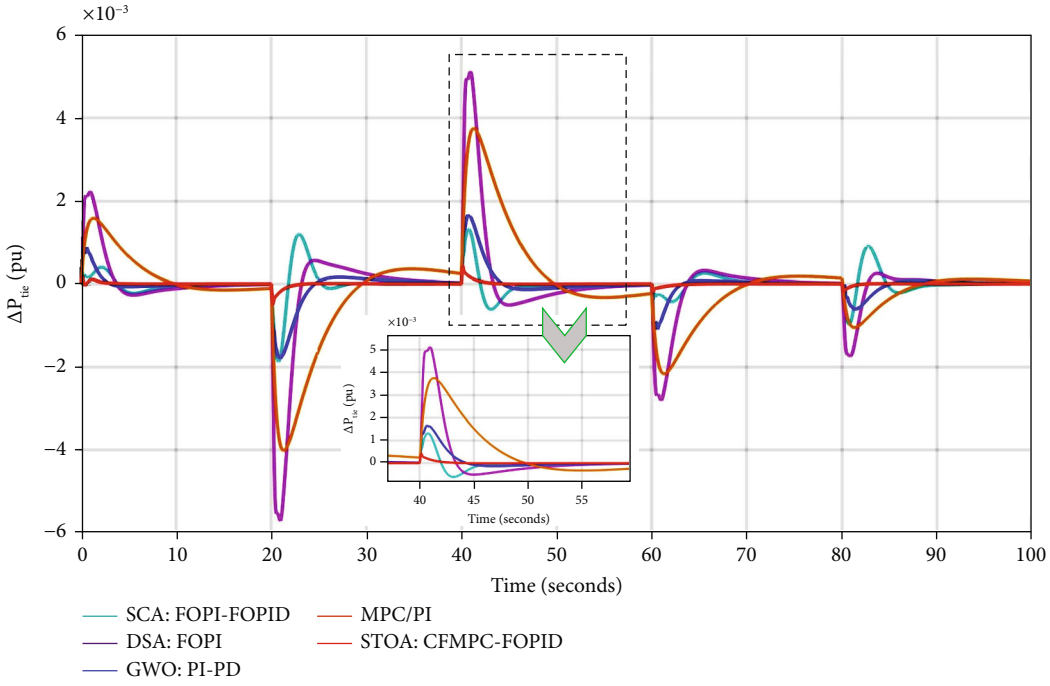

Figure 14: Power sharing response between the two areas under distinct load.

under unbalanced loading [36]. The modelling of the thermal system units is formulated as follows: the power generating capacity of the thermal power plant is 4000 MW operational at 2200 MW at 50 Hz. The governor output $\Delta P_{gi}(s)$ is given by

$$\Delta P_{gi}(s) = \Delta P_{ref}(s) - \frac{1}{R}\Delta f_i(s). \tag{17}$$

The ΔP_{ref} is the reference power and Δf_i is the change in frequency, while droop is presented by $1/R$.

The governor, turbine, and reheater are translated into transfer function denoted by

$$G_{gov}(s) = \frac{0.8 - (0.2/\pi)s}{1 + sT_g}, \tag{18}$$

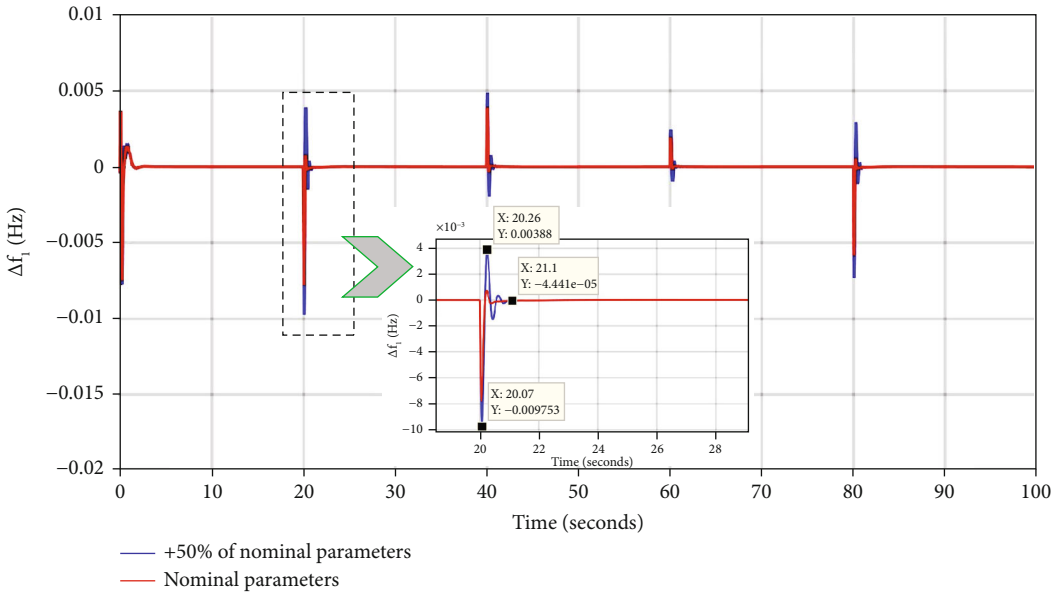

Figure 15: +50% parameter variation response of area-1.

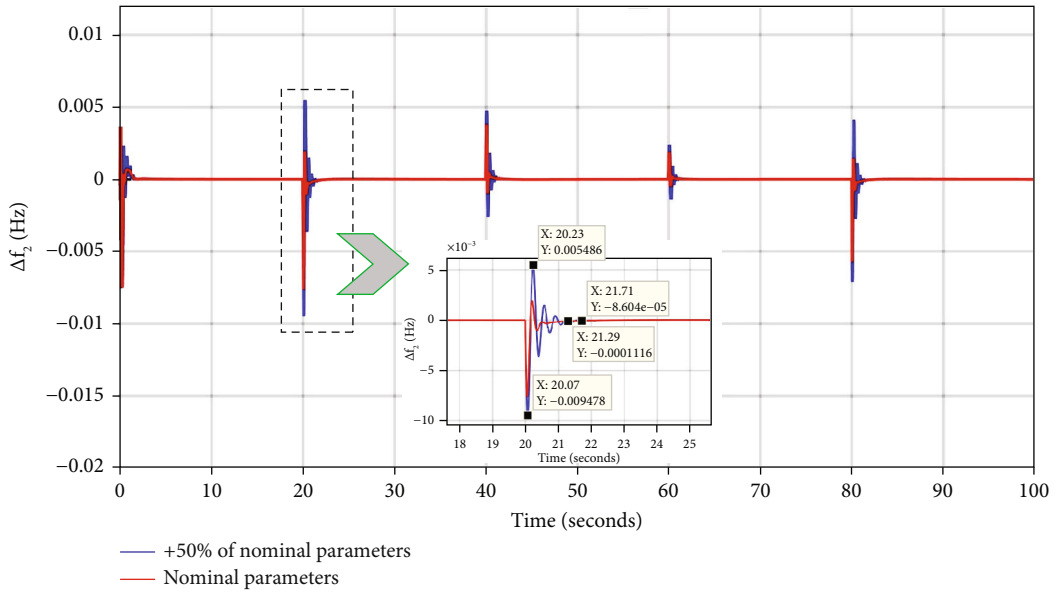

Figure 16: +50% parameter variation response of area-2.

$$G_t(s) = \frac{K_t}{1 + sT_g}, \tag{19}$$

$$G_r(s) = \frac{1 + sK_rT_r}{1 + sT_r}. \tag{20}$$

The generator of the thermal power plant is denoted by the transfer function written in

$$G_{\text{gen}}(s) = \frac{K_p}{1 + sT_p}. \tag{21}$$

In multiarea, the area central error (ACE) is stated by

$$\text{ACE}_i = B_i \Delta f_i + \Delta \text{Tie}_{ij}, i \neq j, \tag{22}$$

where B_i represents the frequency bias factor parameter.

3. Control Implementation

The main concern is to design an efficient controller to abate the ACE signal to zero in order to suppress the frequency deviation and tie-line power variations. This paper tends to rivet the attention towards a novel design of a controller that is a combination of model predictive controller (MPC)

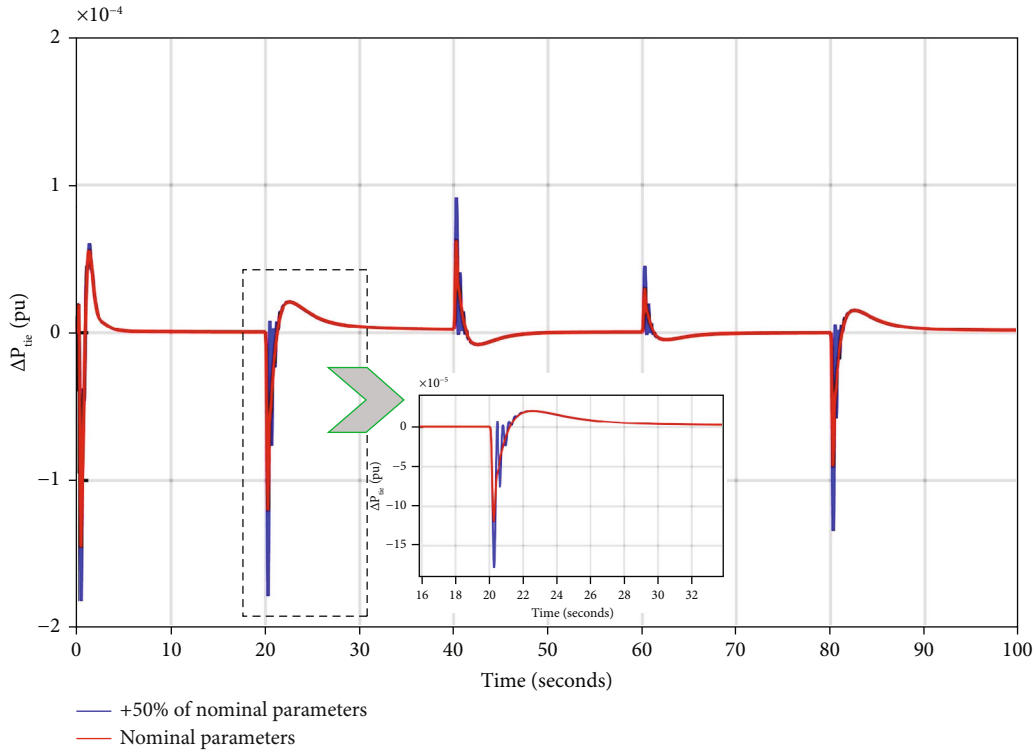

Figure 17: +50% parameter variation response of tie-line.

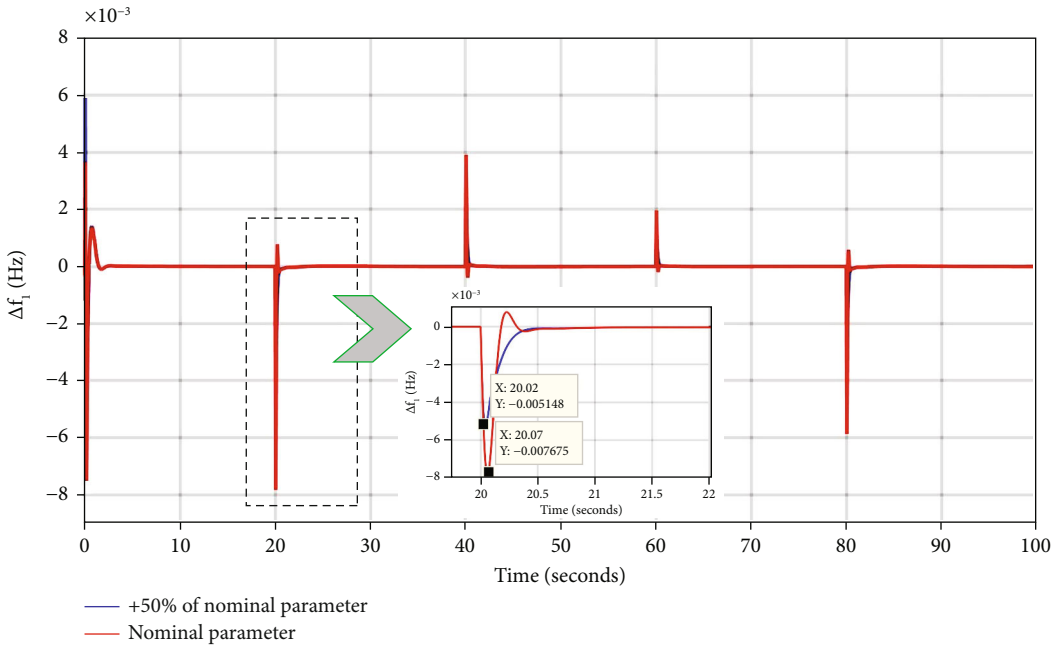

Figure 18: -50% parameter variation response of area-1.

which is supervising an ACE signal, while there is dual FOPID controller with the name FOPID-1 refining the signal received from the output frequency of respective area; the corresponding summation of the two controller response, i.e., MPC and FOPID-1, is transferred to FOPID-2 which completes the overall cascaded structure of the proposed CFMPC-FOPID controller. The proposed controller parameters are optimized by STOA search algorithm to extract optimal parameters for the controller. The overall design provides better control in ameliorating the system

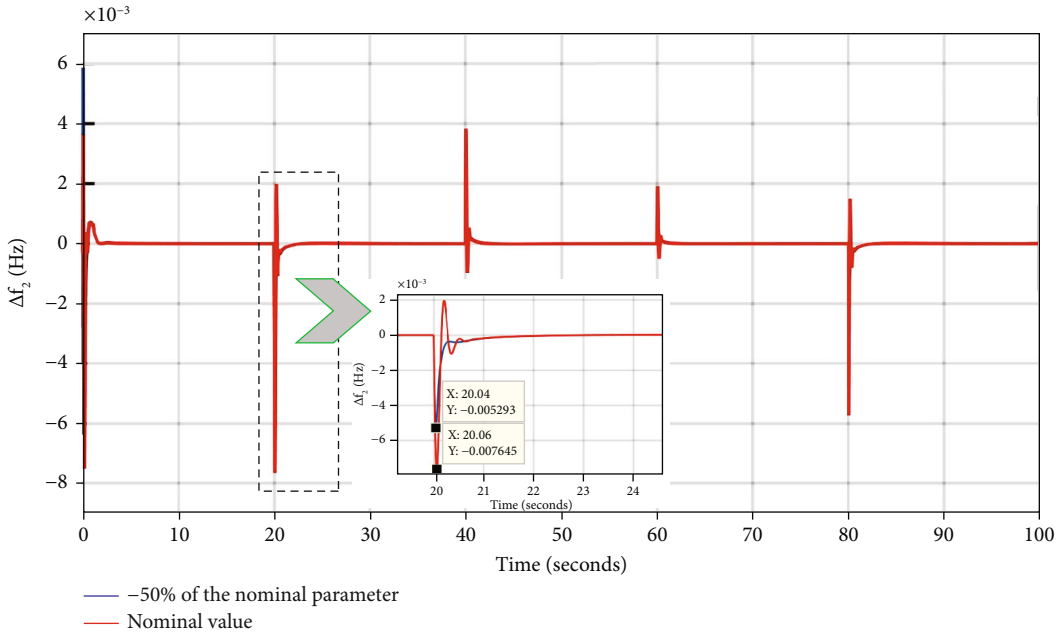

Figure 19: -50% parameter variation response of area-2.

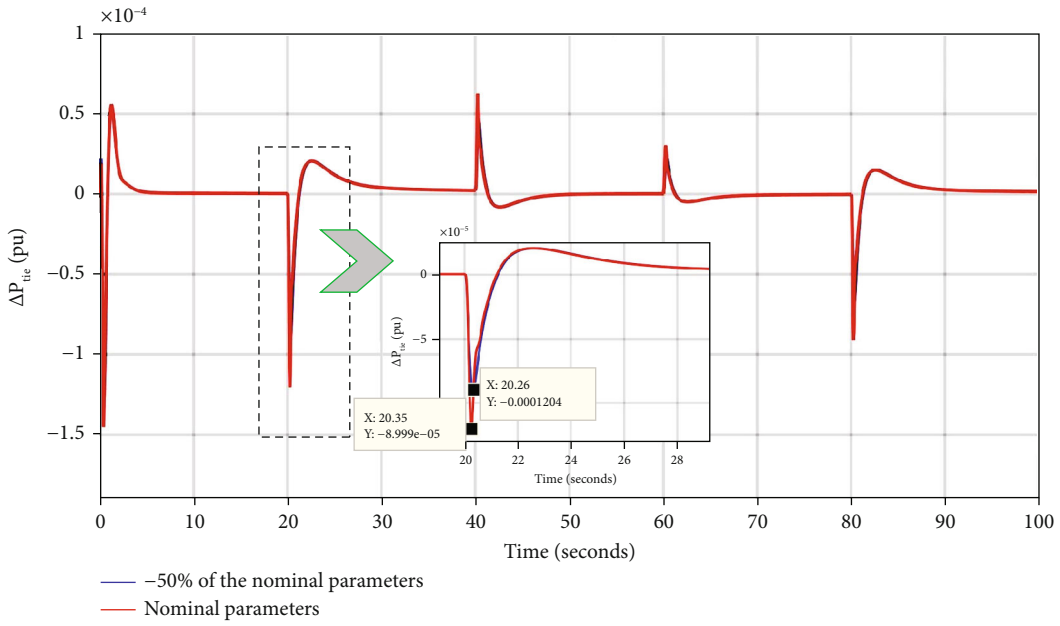

Figure 20: -50% parameter variation response of tie-line.

Table 6: System parameter variation analysis.

Controllers	Area-1			Area-2			Tie-line (puMW)			ITAE
	O.S (Hz)	U.S (Hz)	Time (s)	O.S (Hz)	U.S (Hz)	Time (s)	O.S (pu) 10^{-5}	U.S (pu) 10^{-5}	Time (s)	
Proposed	0.00103	0.00791	1.1	0.00218	0.00762	1.29	3.18	8.99	10	0.0021
Proposed (+50%)	0.00388	0.00975	1.1	0.00548	0.00947	1.29	3.19	17.6	10	0.0048
Proposed (-50%)	0	0.0051	0.438	0	0.00529	1.03	3.18	12.02	10	0.0018

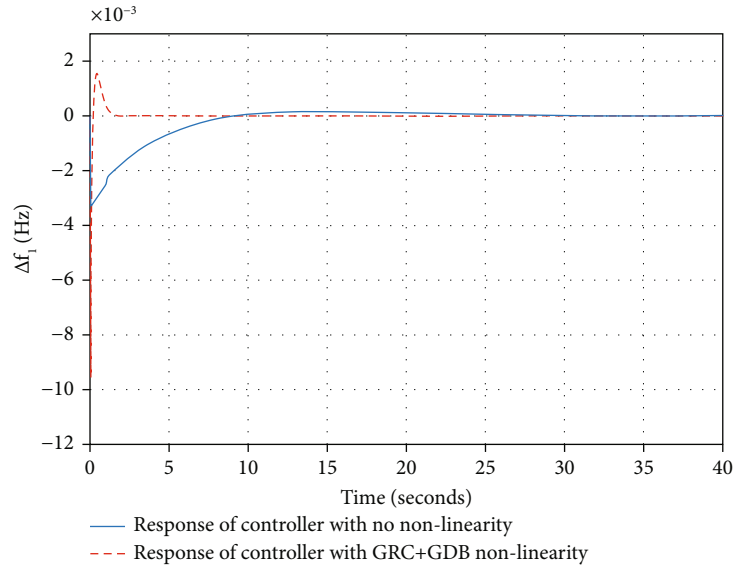

(a)

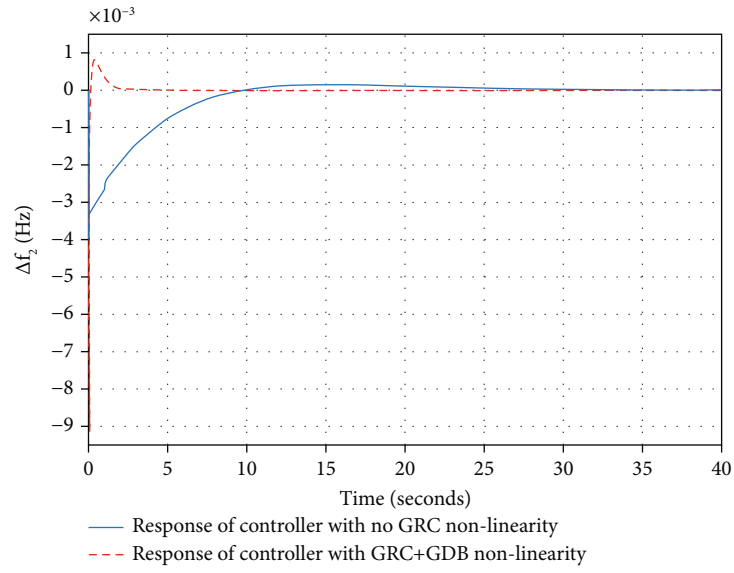

(b)

Figure 21: With and without nonlinearity responses: (a) Δf_1 and (b) Δf_2.

stability by curbing the frequency deviation under different conditions in the power system. The control formation is shown in Figure 4.

3.1. FOPID Controller. In recent times, the importance of FOPID controller has gained an engrossing attention due to its simplicity and better control ability as compared to conventional PID controller. The FOPID controller is interpreted into transfer function as given by

$$G(s) = K_P + \frac{K_I}{S^{\lambda}} + K_D s^{\mu}. \quad (23)$$

In equation (23), the parameters K_P, K_I, and K_D are denoting the gains of the FOPID controller. In addition, λ and μ define as integrator and differentiator fractional parameters, where λ and μ are limited between 0 and 1 which enhances the ability over conventional PID controller by purifying the tuning. The addition of FOPID-1 and FOPID-2 tunable parameters is listed in

$$X_i(t) = \left[K_{p1}, K_{I1}, K_{D1}, \lambda_1, \mu_1, K_{P2}, K_{I2}, K_{D2}, \lambda_2, \mu_2\right] \quad (24)$$

3.2. MPC Control Implementation. The MPC is a modern control theory that relies on forecasting to solve problems, and it is heavily utilized in industrial operations. The MPC defining characteristics include the capacity to address restrictions, compensation for the delays in the system, online optimization, and numerous interpretations of

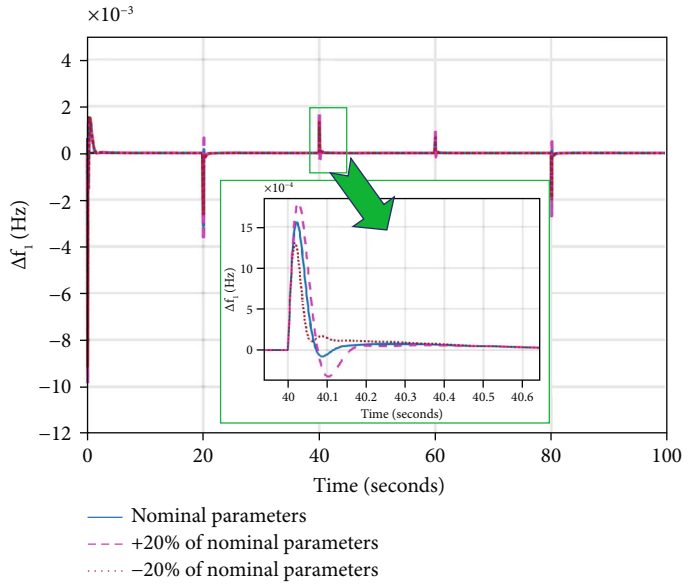

(a)

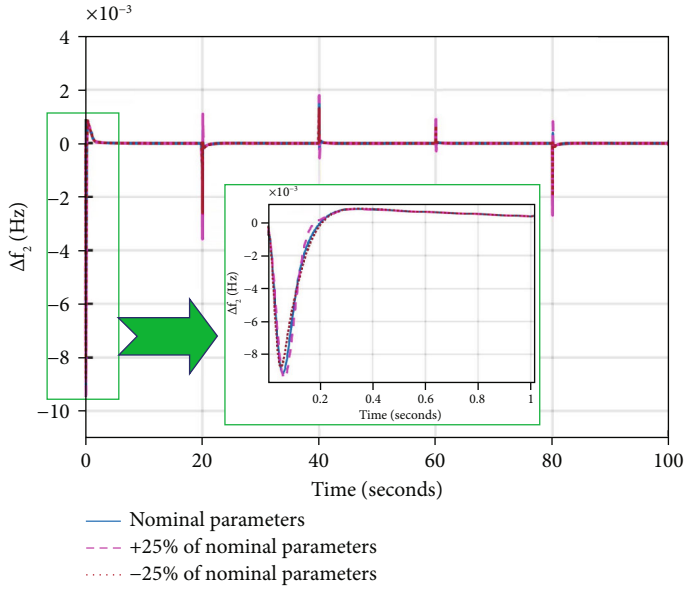

(b)

Figure 22: Continued.

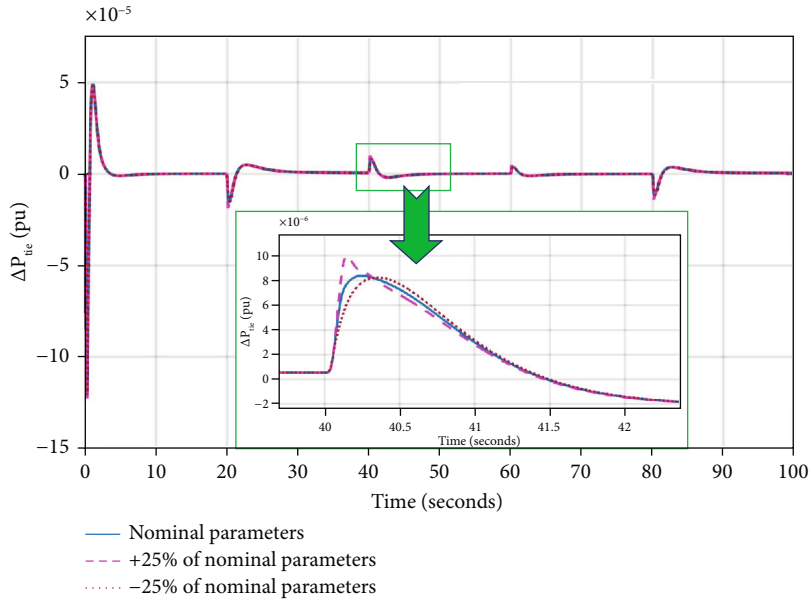

(c)

Figure 22: Sensitivity analysis at ±25% change in nominal values: (a) Δf_1, (b) Δf_2, and (c) ΔP_{tie}.

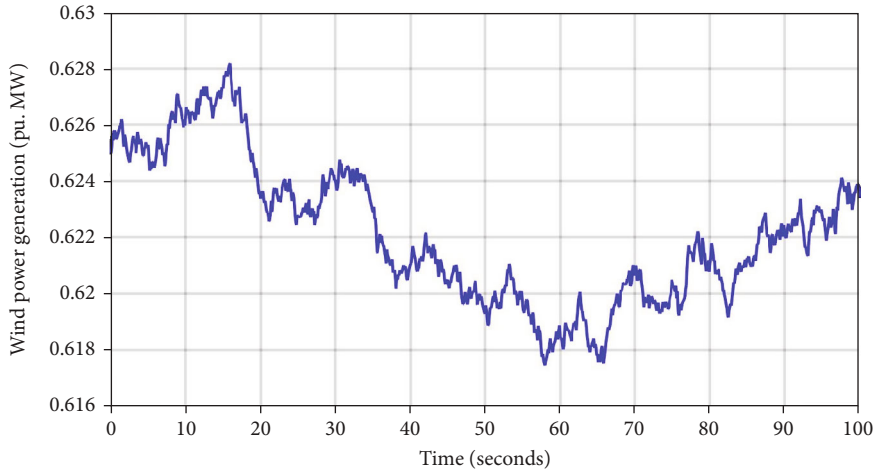

Figure 23: Wind power output.

variables [41]. A controller and a prediction unit make up the MPC; furthermore, the prediction unit extrapolates the system's potential from its output to the future. The control module reduces the predicted output in order to minimize the controlled fitness equation. The fitness equality may be simplified when there are system limits by using the output estimation unit through the use of the control element [33]. The control plant input and output are written as

$$x(k+1) = Ax(k) + BS_i u_p(k), \tag{25}$$

$$y(k) = s_o^{-1} Cx(k) + s_o^{-1} DS_i u_p(k). \tag{26}$$

From equations (25) and (26), A, B, C, and D denote the constant state space matrices, and S_0 and S_i are representing the diagonal matrices of the input and output scale factor, respectively. The u_p represents the dimensionless vector.

$$x(k+1) = Ax(k) + B_u(k) + B_v v(k) + B_d d(k), \tag{27}$$

$$y(k) = Cx(k) + D_v v(k) + D_d d(k), \tag{28}$$

where $u(k)$ is the input signal and $x(k)$ is the system state, $v(k)$ is a measurable turbulence, $d(k)$ is an unmeasured disruption, $y(k)$ is the system outputs, B_u, B_v, and B_d are the equivalent columns of BS_i, and the D_v and D_d are

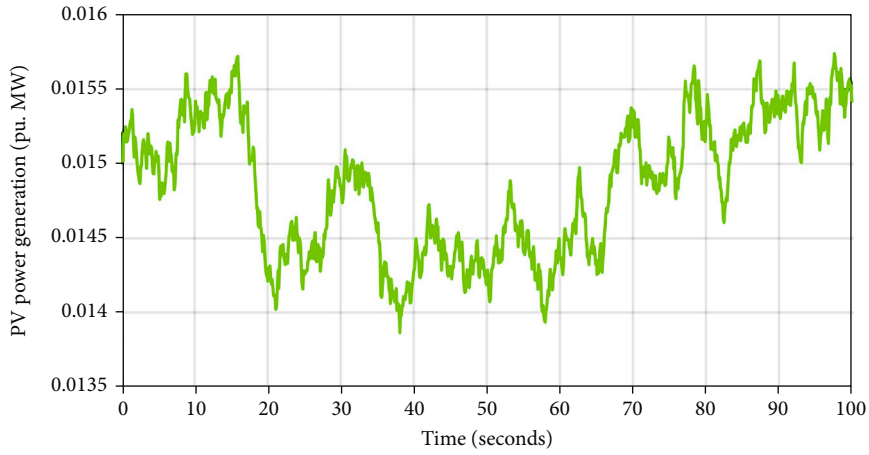

FIGURE 24: PV power output response.

the corresponding columns of $s_o^{-1}DS_i$. The cost function of MPC is given by

$$\min_{\Delta u(k),\cdots,\Delta u(k+M-1)}\left\{\sum_{j=0}^{m-1}\Delta u^T(k+j)R\Delta u(k+j) + \sum_{i=0}^{P-1}\Delta y^T(k+i)Q\Delta y(k+i)\right\}. \tag{29}$$

Here, Q and R are the weighting vectors for balancing the square future control and performance predictive error, where control and prediction horizons are depicted by M and P and sample time is denoted by T.

3.3. Sooty Tern Optimizer Algorithm. In 2019, Dhiman and Kaur have introduced the sooty tern optimization algorithm (STOA) [42]. Sooty terns (ST) are sea birds that may be found all over the globe; they are huge species with a range of sizes and masses. They eat fish, insects, amphibians, earthworms, and various reptiles. ST use bread crumbs as fish bait and made a rain sound with their feet to coax earthworms out of hiding. They like communal living, and they use cunning to stalk and ambush their victim. Migration and assault on prey are major aspects of the behavior of ST. Immigration is described as the seasonal travel of this bird in search of food that gives energy. They travel and migrate as a cluster to escape shocks; thus, their beginning places may vary. ST migrate towards the strongest and most powerful ST in the cluster, while other returns to their original places. ST must avoid collisions through immigration, as stated in [43]

$$\vec{C}_{\text{st}} = S_A \times \vec{P}_{\text{st}}(z), \tag{30}$$

$$S_A = C_f - \left(z \times \left(\frac{C_f}{\text{Iter}_{\max}}\right)\right), \tag{31}$$

where $\vec{C}_{\text{st}}$ defines the ST position that does not encounter with another ST position, $\vec{P}_{\text{st}}$ is the present ST location, z denotes the current iteration, S_A is the ST motion in a given search region, and C_f is a regulating variable to alter S_A. Following equation (32), the ST is congregated with better neighbors after avoiding collision.

$$\vec{M}_{\text{st}} = C_B \times \left(\vec{P}_{\text{bst}}(z) - \vec{P}_{\text{st}}(z), \tag{32}$$

$$C_B = 0.5 \times R_{\text{and}}, \tag{33}$$

where $\vec{M}_{\text{st}}$ indicates the different locations of a ST, $\vec{P}_{\text{bst}}$ is the best of ST, C_B signifies a random variable, and R_{and} is a random number in the interval [0, 1]. The location of the ST can be adjusted as

$$\vec{D}_{\text{st}} = \vec{C}_{\text{st}} + \vec{M}_{\text{st}}. \tag{34}$$

$\vec{D}_{\text{st}}$ demonstrates the distinction between the ST and the ST with the best fitness. The ST exhibit helical motion in the air, as shown in

$$\acute{x} = R_{\text{adi}} \times \sin(i), \tag{35}$$

$$\acute{y} = R_{\text{adi}} \times \cos(i), \tag{36}$$

$$\acute{z} = R_{\text{adi}} \times i, \tag{37}$$

$$r = u \times e^{kv}, \tag{38}$$

where R_{adi} signifies the radius of every helical turn, i is a factor in the interval $[0 \le k \le 2]$, u and v provide the helical shape constant, and e is the natural logarithm. The ST location can be updated by

$$\vec{P}_{\text{st}}(z) = \vec{D}_{\text{st}} \times (\acute{x} + \acute{y} + \acute{z}) \times \vec{P}_{\text{bst}}(z), \tag{39}$$

where $\vec{P}_{\text{st}}(z)$ regulates the locations of other sooty terns while maintaining the optimal outcome. The block diagram of STOA is exhibited in Figure 5. The STOA is adopted to

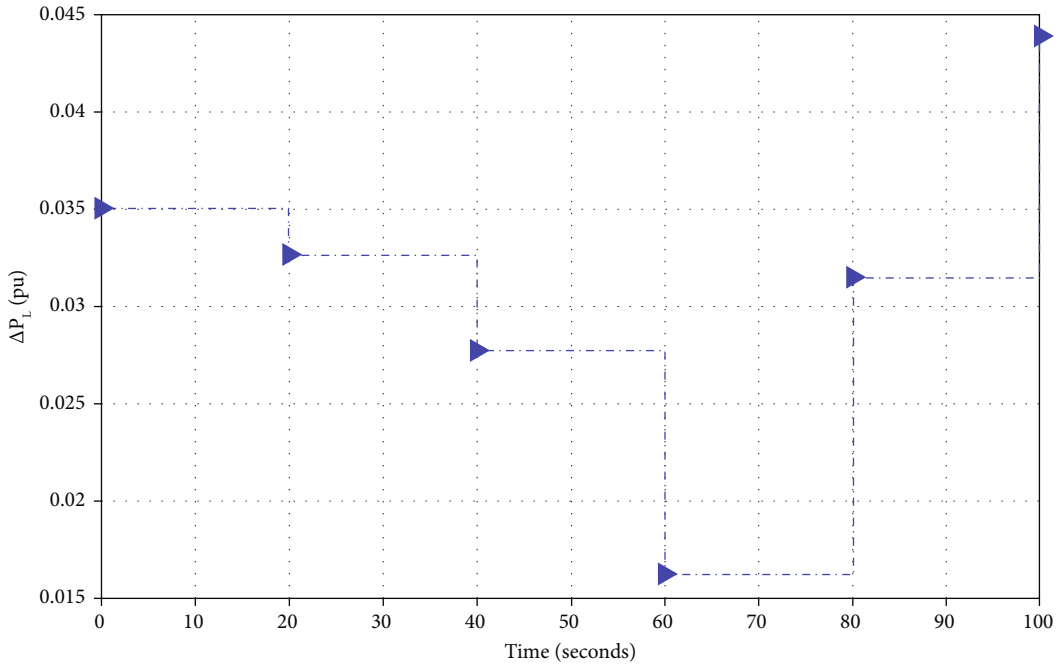

(a)

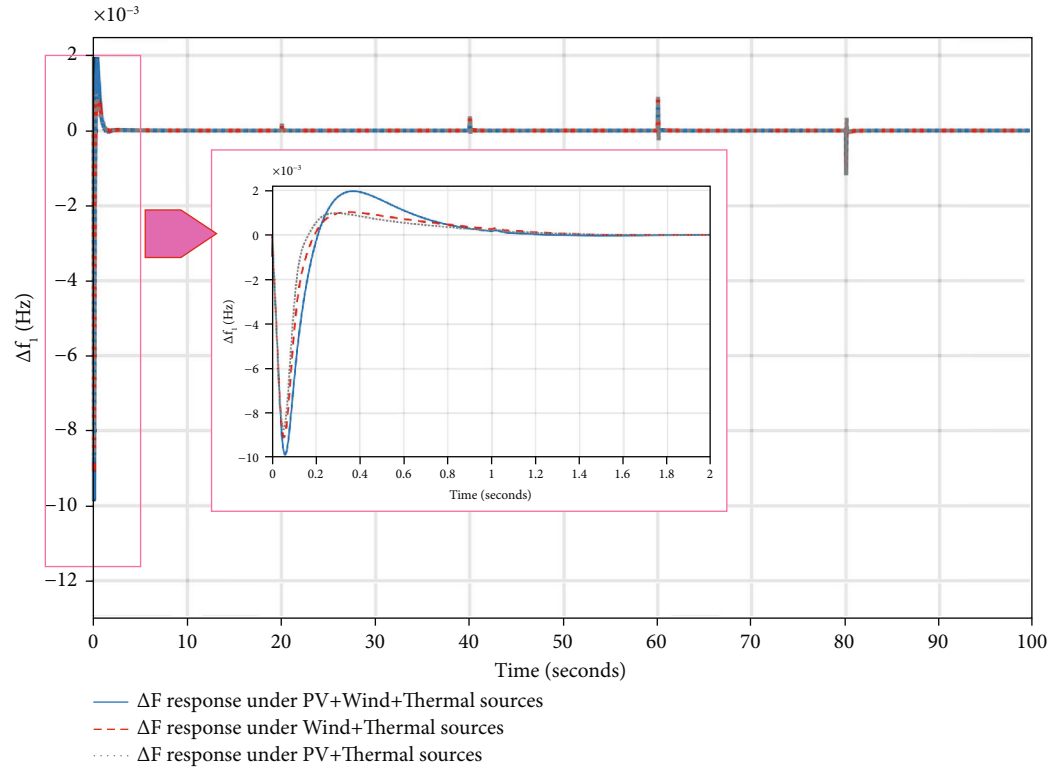

(b)

Figure 25: Continued.

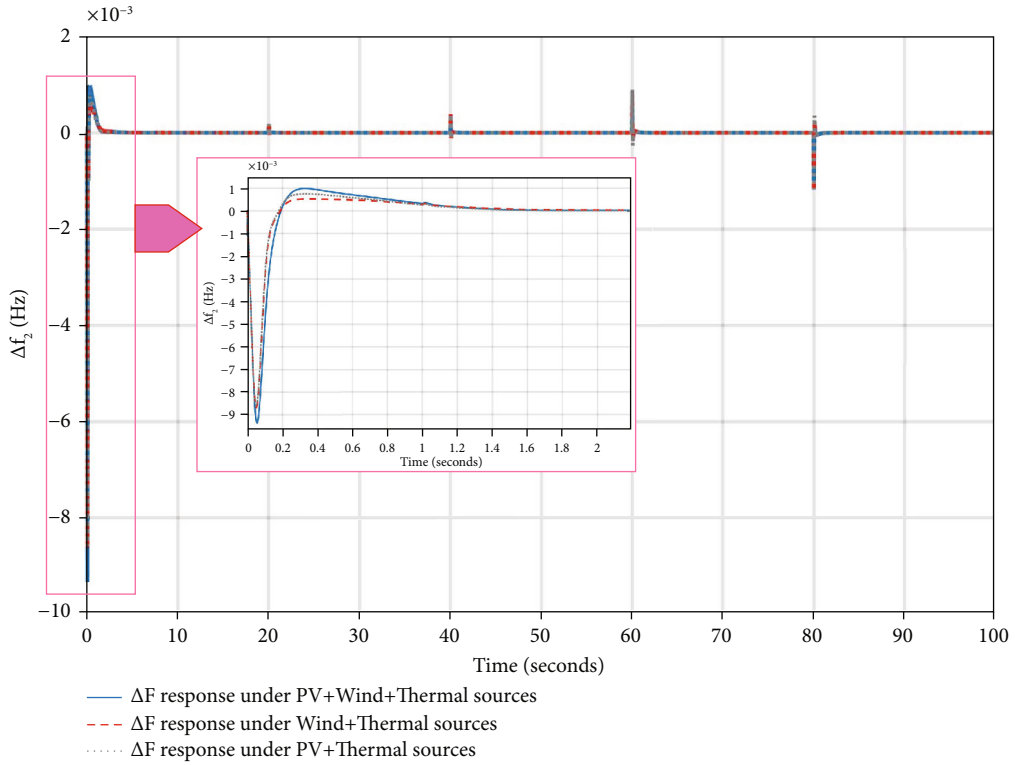

(c)

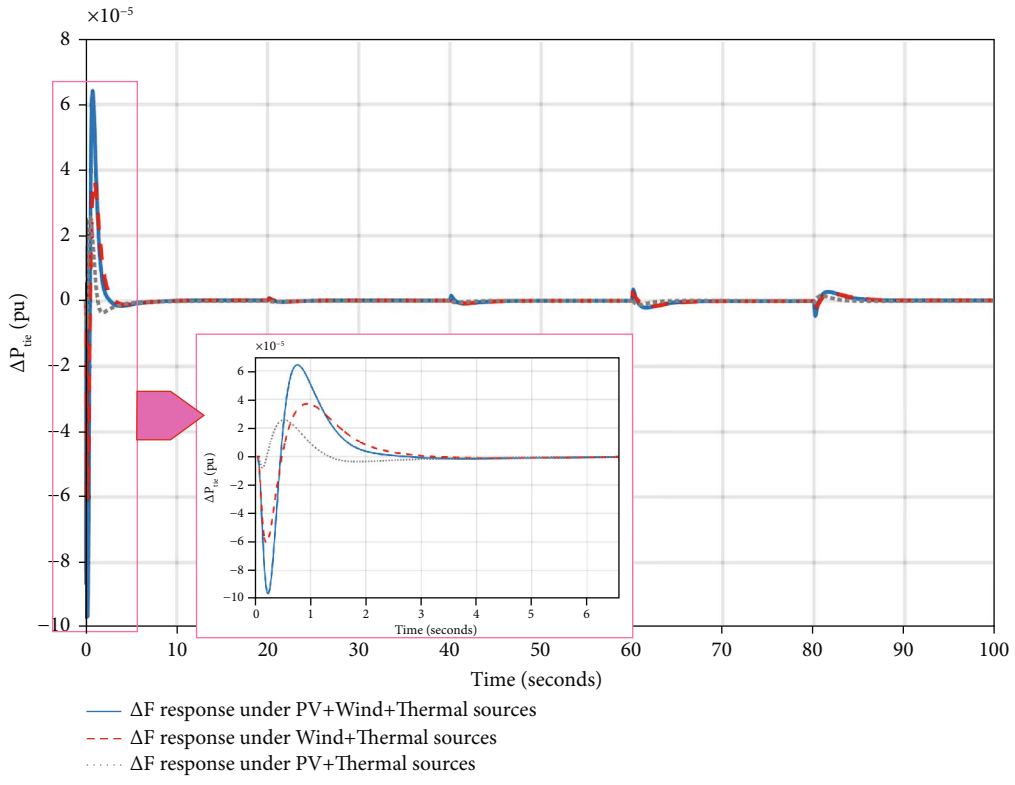

(d)

Figure 25: CFMPC-FOPID responses under different generating sources: (a) ΔP_L, (b) Δf_1, (c) Δf_2, and (d) ΔP_{tie}.

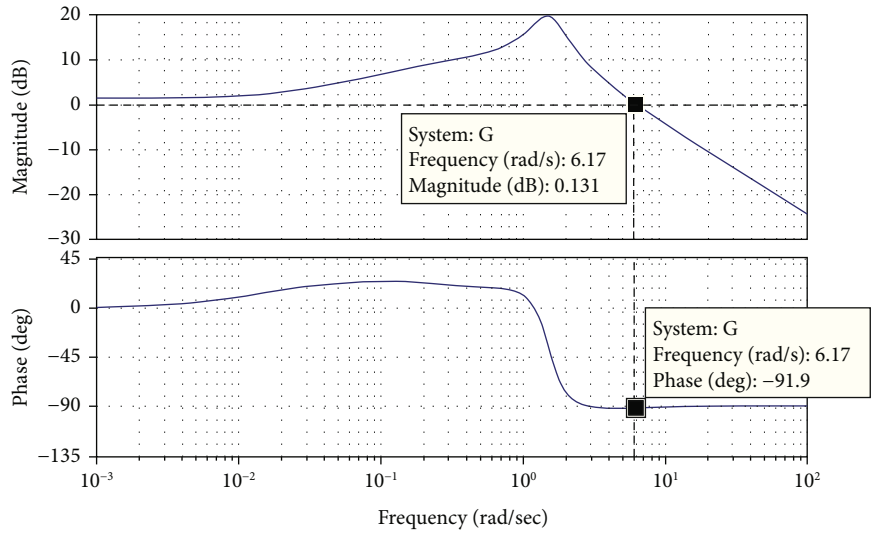

Figure 26: Power system stability response analysis.

optimize the CFMPC-FOPID controller parameters while considering the fitness function (ITAE) as demonstrated in

$$\text{ITAE} = \int_0^{\infty} t(|\Delta f_1| + |\Delta f_2| + |\Delta P_{\text{tie}}|)\text{dt}. \tag{40}$$

The convergence mobility of the optimizing algorithm is shown in Figure 6.

The optimal parameter generated by the STOA after 100 iterations is enumerated in Table 1.

4. Result Outcome

The performance and effectiveness of the proposed work are visualized in this section. The efficiency of the suggested control technique in multiarea hybrid power electrical system is tested by applying four different scenarios: (i) applying similar load patterns in both areas, (ii) applying different load patterns in both areas, (iii) analysis of the suggested controller under uncertainty in the power system parameters, and (iv) nonlinearities and sensitivity analysis.

4.1. Similar Load Pattern in Multiarea. The controller performance under the similar load pattern is analyzed in multiarea power system that comprises of PV and wind energy sources. The fluctuating load pattern is depicted in Figure 7. Against the similar applied load, the controller frequency response in area-1 and area-2 is exhibited in Figures 8 and 9, respectively.

The tabular study of the responses of the controllers under changing load condition is observed. The controller response at Point-A, Point-B, and Point-C on graph is chosen to monitor the performance of the controllers in area-1 which is presented in Table 2. The findings clearly demonstrate that the suggested controller outperforms the alternatives in terms of response robustness. The proposed controller (CFMPC-FOPID) has shown a settling time of 1.21 sec, 0.727 sec, and 0.689 sec for Point-A, Point-B, and Point-C, respectively. The undershoot (U.S) response of the CFMPC-FOPID controller is 0.0068 and 0.0062 in case of Point-A and Point-B, while at Point-C, the U.S response of the controller is zero. Similarly, the overshoot (O.S) response of the CFMPC-FOPID controller for Point-A, Point-B, and Point-C for area-1 is 0.0031, 0, and 0.0032, respectively.

Besides this, Table 3 evaluates the performance of the controllers in area-2. Compared to previous controllers, the frequency response analysis indicates that the proposed controller has successfully reduced the frequency of abrupt reaction times. The reaction time of the suggested controller is 1.79 sec for Point-A, 0.651 sec for Point-B, and 0.86 sec for Point-C in Figure 9.

The power exchange pattern (tie-line) between the two areas is presented in Figure 10. The exchange of power response of the proposed controller is robust as compared to other controllers. The proposed controller is showing minute fluctuation in power curve with respect to other controllers.

4.2. Distinct Load Patterns in Multiarea. Keeping in view the real-world scenarios and practical load conditions is vital to claim the capability of the proposed work. The load of any area can vary, and it can vary on dissimilar fashion, i.e., the fluctuation in load of area-1 cannot be similar to an area-2. Therefore, the distinct load changing pattern is applied on different areas as shown in Figure 11. Against the distinct load condition, the response of area-1 and area-2 is showcased in Figures 12 and 13, respectively. The result depicts that the proposed controller shows robust control ability in restraining the frequency to its pivot position. The S.T of the proposed controller is 1.34 sec, 0.601 sec, and 0.410 sec for Point-A, Point-B, and Point-C, respectively, as highlighted on the graph for area-1. The U.S response of the CFMPC-FOPID controller is 0.0077 and 0.006 in case of Point-A and Point-B, while at Point-C, the U.S response of the controller is zero. Similarly, the O.S response of the CFMPC-FOPID controller for Point-A, Point-B, and Point-C for area-1 is 0.0038, 0, and 0.0031, respectively.

The performance of all the controllers is further tested by applying distinct load in both areas. The performance of the controllers is noted in Table 4.

Similarly, for area-2, the performance of all the controllers is evaluated under the distinct applied load. The tabular results of the controller are highlighted in Table 5. The settling time of the CFMPC-FOPID controller is 1.401 sec for Point-A, 0.891 sec for Point-B, and 0.560 sec for Point-C. The proposed controller shows fast settling time in restraining the frequency.

The tie-line response during the distinct load conditions in each area is shown in Figure 14. It is evident from the response that the proposed controller is performing efficiently over other controllers and showing better power flow.

4.3. Controller Analysis under Uncertainty in the System Parameters. Considering the hybrid power system that comprises of PV and wind power generation units and due to uncertainty in the power plant, the performance of the controller is tested. In this research work, a ±50% variation is applied in governor parameter of the thermal power plant to monitor the control and settling performance of the controller. For the +50% variation in the thermal power plant, the performance of the controller is depicted in Figure 15 for area-1, Figure 16 for area-2, and tie-line power response in Figure 17. The nominal settling time of frequency is 1.1 sec and 1.29 sec in area-1 and area-2.

Keeping the preceding discussion in view, the -50% variation is applied in the thermal system parameter, and the performance of the controller is simulated in Figures 18–20 of area-1, area-2, and tie-line, respectively.

The analysis of system parameter variations is summarized in Table 6.

4.4. Evaluation of Nonlinearities and Sensitivity Response Analysis. The dead band of the speed governor has a significant impact on the efficiency of the power system. The analyzed system becomes nonlinear after the GDB is incorporated into it. Before a shift in valve position triggers an oscillatory response in the system, the GDB slows things down. In the investigation of the proposed controller response, the backlash nonlinearity is set to 0.05% for the thermal power system. Similarly, the rate of change in generating power has a maximum and a minimum that must be respected in practice. The generation rate constraint (GRC) restricts the power generation when it reaches the maximum value. During designing of the thermal power system, the GRC is set at value 0.002 pu MW sec^{-1}. The response of the designed controller under the nonlinearity for the area-1 and area-2 is shown in Figure 21. Moreover, the sensitivity response analysis is conducted for CFMPC-FOPID controller to verify the robustness of the designed controller. The system parameter deviations are applied with ±25% change in the nominal parameters of the power system. The sensitivity response is revealed in Figure 22.

4.5. Generation Response and Its Impact. In this research work, the penetration of renewable into the thermal power system is implemented in knowing the importance of RES which is inevitable. The performance of CFMPC-FOPID is crucial to be analyzed under a combined renewable-based power system. The generation response of the wind power output is shown in Figure 23, while PV power generation is depicted in Figure 24. The overall impact analysis of the renewable into the power system and the performance of the proposed controller in an AGC-deregulated environment is investigated in Figure 25.

Lastly, the stability response of the power system under the proposed controller is depicted in Figure 26. From the stability response (bode plot), it is conspicuous that the overall system remains stable under the designed controller.

5. Conclusion

This research paper has intended to present an innovative design method to counter the load frequency control problem in multiarea hybrid power system. To ensure the operation of the proposed controller under high penetration of renewable sources into the power network, the power system is composed of renewable energy sources (PV and wind). For the stable operation of the power system, a modified cascaded structure design is proposed. The proposed controller is a combination of MPC, FOPID-1, and FOPID-2 collectively summarized as CFMPC-FOPID. The major formulation of MPC is to minimize the area control error, while FOPID-1 is refining the signal, entering from output frequency of an area and their collective sum, i.e., MPC and FOPID-1 are fed to FOPID-2. The CFMPC-FOPID is optimized by a sooty tern optimization algorithm for extraction of best parameters of the recommended controller. Moreover, to proclaim an effectiveness of the proposed controller, the designed work is passed through number of testing scenarios like similar load variations in multiarea, distinct load variations in multiarea, uncertainty in the parameters of the power system, nonlinearities in the power system, and sensitivity analysis. The outcomes encapsulate that the proposed controller has robust ability to restrain the frequency in range between 0.41 sec and 1.79 sec in multiarea power system.

For the future studies, complex interconnected model analysis and their performance under changing load can be explored.

Abbreviations

B: Frequency bias factor (puMW/Hz)
R: Droop characteristics of governor speed
T_i: Time constant (sec) for i parameter (governor, turbine, power system, and reheat)
K_i: Gain for i parameter (governor, turbine, power system, and reheat)
G_i: Transfer function of i parameter
ρ: Air density (kg/m^3)
C_p: Power coefficient
β: Blade pitch angle (deg)
a: Swept area (m^2)
V_m: Wind speed (m/s)
Δf_i: Deviation in frequency (Hz) in i area
ΔP_{tie}: Tie-line power (puMW)

TSR: Turn speed ratio
ACE: Area control error
LFC: Load frequency control
MPP: Maximum power point
STOA: Sooty tern optimization algorithm
CFMPC: Cascaded fractional model predictive controller
FOPID: Fractional-order PID controller
ITAE: Integral time-multiplied absolute error
RES: Renewable energy sources.

Data Availability

No underlying data was collected or produced in this study.

Disclosure

Muhammad Khalid's present address is King Fahd University of Petroleum & Minerals, Dhahran 31261, Saudi Arabia.

Conflicts of Interest

The authors of this paper have no known conflict or any other financial interest that could affect the outcome of this paper.

Acknowledgments

This publication is based upon work supported by the King Fahd University of Petroleum and Minerals. The authors at KFUPM acknowledge the Interdisciplinary Research Center for Renewable Energy and Power Systems for the support received under grant no. EC221008. Also, Muhammad Khalid would like to acknowledge the support from the SDAIA-KFUPM Joint Research Center for Artificial Intelligence (JRC-AI).

References

[1] W. Gorman, S. Jarvis, and D. Callaway, "Should I stay or should I go? The importance of electricity rate design for household defection from the power grid," *Applied Energy*, vol. 262, article 114494, 2020.

[2] A. K. Barik, S. Jaiswal, and D. C. Das, "Recent trends and development in hybrid microgrid: a review on energy resource planning and control," *International Journal of Sustainable Energy*, vol. 41, no. 4, pp. 308–322, 2022.

[3] M. M. Gulzar, M. Iqbal, S. Shahzad, H. A. Muqeet, M. Shahzad, and M. M. Hussain, "Load frequency control (LFC) strategies in renewable energy-based hybrid power systems: a review," *Energies*, vol. 15, no. 10, p. 3488, 2022.

[4] H. Abubakr, J. M. Guerrero, J. C. Vasquez et al., "Adaptive LFC incorporating modified virtual rotor to regulate frequency and tie-line power flow in multi-area microgrids," *IEEE Access*, vol. 10, pp. 33248–33268, 2022.

[5] G. Magdy, G. Shabib, A. A. Elbaset, and Y. Mitani, "Optimized coordinated control of LFC and SMES to enhance frequency stability of a real multi-source power system considering high renewable energy penetration," *Protection and Control of Modern Power Systems*, vol. 3, no. 1, pp. 1–15, 2018.

[6] M. M. Gulzar, D. Sibtain, A. F. Murtaza, S. Murawwat, M. Saadi, and A. Jameel, "Adaptive fuzzy based optimized proportional-integral controller to mitigate the frequency oscillation of multi-area photovoltaic thermal system," *International Transactions on Electrical Energy Systems*, vol. 31, no. 1, article e12643, 2021.

[7] M.-R. Chen, G.-Q. Zeng, and X.-Q. Xie, "Population extremal optimization-based extended distributed model predictive load frequency control of multi-area interconnected power systems," *Journal of the Franklin Institute*, vol. 355, no. 17, pp. 8266–8295, 2018.

[8] B. Mohanty, S. Panda, and P. K. Hota, "Differential evolution algorithm based automatic generation control for interconnected power systems with non-linearity," *Alexandria Engineering Journal*, vol. 53, no. 3, pp. 537–552, 2014.

[9] B. Mohanty, S. Panda, and P. K. Hota, "Controller parameters tuning of differential evolution algorithm and its application to load frequency control of multi-source power system," *International Journal of Electrical Power & Energy Systems*, vol. 54, pp. 77–85, 2014.

[10] J. Sharma, Y. V. Hote, and R. Prasad, "Robust PID load frequency controller design with specific gain and phase margin for multi-area power systems," *IFAC-PapersOnLine*, vol. 51, no. 4, pp. 627–632, 2018.

[11] Y. V. Hote and S. Jain, "PID controller design for load frequency control: past, present and future challenges," *IFAC-PapersOnLine*, vol. 51, no. 4, pp. 604–609, 2018.

[12] R. Alayi, F. Zishan, S. R. Seyednouri, R. Kumar, M. H. Ahmadi, and M. Sharifpur, "Optimal load frequency control of island microgrids via a PID controller in the presence of wind turbine and PV," *Sustainability*, vol. 13, no. 19, p. 10728, 2021.

[13] R. K. Khadanga, A. Kumar, and S. Panda, "A novel modified whale optimization algorithm for load frequency controller design of a two-area power system composing of PV grid and thermal generator," *Neural Computing and Applications*, vol. 32, no. 12, pp. 8205–8216, 2020.

[14] V. Shanmugasundaram, "Artificial bee colony algorithm based automatic generation control in two-area non-reheat thermal power system using SMES," in *2017 IEEE International Conference on Power, Control, Signals and Instrumentation Engineering (ICPCSI)*, pp. 2126–2130, Chennai, India, 2017.

[15] N. Paliwal, L. Srivastava, and M. Pandit, "Jaya algorithm based optimal design of LQR controller for load frequency control of single area power system," in *Social Networking and Computational Intelligence*, pp. 595–603, Springer, Singapore, 2020.

[16] K. S. Rajesh and S. S. Dash, "Load frequency control of autonomous power system using adaptive fuzzy based PID controller optimized on improved sine cosine algorithm," *Journal of Ambient Intelligence and Humanized Computing*, vol. 10, no. 6, pp. 2361–2373, 2019.

[17] E. S. Ali and S. M. Abd-Elazim, "Bacteria foraging optimization algorithm based load frequency controller for interconnected power system," *International Journal of Electrical Power & Energy Systems*, vol. 33, no. 3, pp. 633–638, 2011.

[18] K. Ranjitha, P. Sivakumar, R. Elavarasu, and M. Monica, "Load frequency controller based on ant colony and firefly algorithm optimization-a review," *AIP Conference Proceedings*, , no. 1, AIP Publishing LLC, p. 040020, 2022.

[19] S. Kumari and G. Shankar, "A novel application of salp swarm algorithm in load frequency control of multi-area power system," in *2018 IEEE International Conference on Power Electronics, Drives and Energy Systems (PEDES)*, pp. 1–5, Chennai, India, 2018.

[20] S. M. Abd-Elazim and E. S. Ali, "Load frequency controller design of a two-area system composing of PV grid and thermal generator via firefly algorithm," *Neural Computing and Applications*, vol. 30, no. 2, pp. 607–616, 2018.

[21] W. Ding, S. Patnaik, S. Sidhardh, and F. Semperlotti, "Applications of distributed-order fractional operators: a review," *Entropy*, vol. 23, no. 1, p. 110, 2021.

[22] E. Çelik, "Design of new fractional order PI–fractional order PD cascade controller through dragonfly search algorithm for advanced load frequency control of power systems," *Soft Computing*, vol. 25, no. 2, pp. 1193–1217, 2021.

[23] Y. Arya, "Improvement in automatic generation control of two-area electric power systems via a new fuzzy aided optimal PIDN-FOI controller," *ISA Transactions*, vol. 80, pp. 475–490, 2018.

[24] V. Veerasamy, N. I. A. Wahab, R. Ramachandran et al., "A Hankel matrix based reduced order model for stability analysis of hybrid power system using PSO-GSA optimized cascade PI-PD controller for automatic load frequency control," *IEEE Access*, vol. 8, pp. 71422–71446, 2020.

[25] P. Satapathy, M. K. Debnath, and P. K. Mohanty, "Design of PD-PID controller with double derivative filter for frequency regulation," in *2018 2nd IEEE International Conference on Power Electronics, Intelligent Control and Energy Systems (ICPEICES)*, pp. 1142–1147, Delhi, India, 2018.

[26] W. Tasnin, L. C. Saikia, and M. Raju, "Deregulated AGC of multi-area system incorporating dish-Stirling solar thermal and geothermal power plants using fractional order cascade controller," *International Journal of Electrical Power & Energy Systems*, vol. 101, pp. 60–74, 2018.

[27] M. Shouran and A. Alsseid, "Particle swarm optimization algorithm-tuned fuzzy cascade fractional order PI-fractional order PD for frequency regulation of dual-area power system," *PRO*, vol. 10, no. 3, p. 477, 2022.

[28] R. Mohammadikia and M. Aliasghary, "A fractional order fuzzy PID for load frequency control of four-area interconnected power system using biogeography-based optimization," *International Transactions on Electrical Energy Systems*, vol. 29, no. 2, article e2735, 2019.

[29] M. Barakat, "Novel chaos game optimization tuned-fractional-order PID fractional-order PI controller for load–-frequency control of interconnected power systems," *Protection and Control of Modern Power Systems*, vol. 7, no. 1, pp. 1–20, 2022.

[30] M. Bhuyan, D. C. Das, and A. K. Barik, "Proficient power control strategy for combined solar gas turbine-wind turbine generator-biodiesel generator based two area interconnected microgrid employed with DC link using Harris's hawk optimization optimised tilt-integral-derivative controller," *International Journal of Numerical Modelling: Electronic Networks, Devices and Fields*, vol. 35, no. 4, p. e2991, 2022.

[31] K. Singh, M. Amir, and Y. Arya, "Optimal dynamic frequency regulation of renewable energy based hybrid power system utilizing a novel TDF-TIDF controller," *Energy Sources, Part A: Recovery, Utilization, and Environmental Effects*, vol. 44, no. 4, pp. 10733–10754, 2022.

[32] A. M. Ersdal, L. Imsland, and K. Uhlen, "Model predictive load-frequency control," *IEEE Transactions on Power Systems*, vol. 31, no. 1, pp. 777–785, 2016.

[33] M. Gulzar, S. Rizvi, M. Javed, D. Sibtain, and R. S. u. Din, "Mitigating the load frequency fluctuations of interconnected power systems using model predictive controller," *Electronics*, vol. 8, no. 2, p. 156, 2019.

[34] H. H. Ali, A. M. Kassem, M. Al-Dhaifallah, and A. Fathy, "Multi-verse optimizer for model predictive load frequency control of hybrid multi-interconnected plants comprising renewable energy," *Ieee Access*, vol. 8, pp. 114623–114642, 2020.

[35] D. Sibtain, M. M. Gulzar, A. F. Murtaza et al., "Variable structure model predictive controller based gain scheduling for frequency regulation in renewable based power system," *International Journal of Numerical Modelling: Electronic Networks, Devices and Fields*, vol. 35, no. 4, p. e2989, 2022.

[36] M. M. Gulzar, D. Sibtain, A. Ahmad et al., "An efficient design of adaptive model predictive controller for load frequency control in hybrid power system," *International Transactions on Electrical Energy Systems*, vol. 2022, pp. 1–14, 2022.

[37] P. A. Gbadega and A. K. Saha, "Load frequency control of a two-area power system with a stand-alone microgrid based on adaptive model predictive control," *IEEE Journal of Emerging and Selected Topics in Power Electronics*, vol. 9, no. 6, pp. 7253–7263, 2020.

[38] M. Iqbal and M. M. Gulzar, "Master-slave design for frequency regulation in hybrid power system under complex environment," *IET Renewable Power Generation*, vol. 16, no. 14, pp. 3041–3057, 2022.

[39] I. Koley, P. S. Bhowmik, and A. Datta, "Load frequency control in a hybrid thermal-wind-photovoltaic power generation system," in *2017 4th International Conference on Power, Control & Embedded Systems (ICPCES)*, pp. 1–5, Allahabad, India, 2017.

[40] T. Mahto and V. Mukherjee, "Fractional order fuzzy PID controller for wind energy-based hybrid power system using quasi-oppositional harmony search algorithm," *IET Generation, Transmission & Distribution*, vol. 11, no. 13, pp. 3299–3309, 2017.

[41] D. Q. Mayne, "Model predictive control: recent developments and future promise," *Automatica*, vol. 50, no. 12, pp. 2967–2986, 2014.

[42] G. Dhiman and A. Kaur, "STOA: a bio-inspired based optimization algorithm for industrial engineering problems," *Engineering Applications of Artificial Intelligence*, vol. 82, pp. 148–174, 2019.

[43] A. Kumar and S. Suhag, "Effect of TCPS, SMES, and DFIG on load frequency control of a multi-area multi-source power system using multi-verse optimized fuzzy-PID controller with derivative filter," *Journal of Vibration and Control*, vol. 24, no. 24, pp. 5922–5937, 2018.